

Chapter 3

Hydrogen Storage

Aline Léon

3.1	Introduction	82
3.2	Purification of Hydrogen	83
3.3	Compressed Hydrogen (CGH ₂)	84
3.3.1	Characteristics of CGH ₂	84
3.3.2	Hydrogen Compressors	85
3.3.3	Storage of CGH ₂	92
3.3.4	Outlook	93
3.4	Liquid Hydrogen (LH ₂)	93
3.4.1	Characteristics of Liquid Hydrogen	94
3.4.2	Liquefaction of Hydrogen	96
3.4.3	Liquid Hydrogen Storage	100
3.4.4	Liquefaction Cost	100
3.4.5	Outlook	102
3.5	Solid Storage of Hydrogen (SSH ₂)	102
3.5.1	Reversible Storage Systems	103
3.5.2	Irreversible Storage Systems	117
3.5.3	Outlook	121
3.6	Conclusions	121
	Notes	120
	References	123

List of Abbreviations

CGH ₂	Compressed Hydrogen
CUTE	Clean Urban Transportation Europe
EU	European Union
LH ₂	Liquid Hydrogen
SSH ₂	Solid Storage of Hydrogen

Aline Léon

Institut für Nanotechnologie, Forschungszentrum Karlsruhe, P.O. Box 3640, D – 76021 Karlsruhe, Germany, e-mail: aline.leon@int.fzk.de

3.1 Introduction

For the development of the future hydrogen economy, a safe and efficient means of storing hydrogen is required in mobile, portable, and stationary applications. Cars represent the ultimate market for manufacturers of hydrogen storage systems, although they pose some of the greatest challenges to commercialization due to their relatively small size, the necessity for a vast fuelling infrastructure, and public acceptance. In addition, performance and reliability are high and the cost issue is critical. Indeed, for a successful application of hydrogen as an energy carrier, hydrogen should be stored safely for variable periods of time, as efficiently as gasoline. At the same time, simple handling and low costs should be ensured. However, the unusual physical and thermodynamic properties of hydrogen today pose the greatest technological challenges to its penetration in the market as an energy carrier.

The phase diagram of hydrogen, Fig. 3.1, indicates that the three phases coexist at a temperature of 13.803 K. The solid phase exists below 14 K. The liquid phase is present from the triple point up to the critical point. The boiling temperature of hydrogen at 1 bar is around 20 K. Above the critical point ($T_c = 32.976$ K and $P_c = 12.928$ bar), the liquid – vapor equilibrium ceases to exist. Therefore, hydrogen is in the gas phase at normal pressure (1 bar) and temperature (298.15 K).

Under normal conditions, the density of the gas is 0.08238 Kg/m^3 [1]. For 5 kg of hydrogen, this implies a volume of around 60 m^3 and an energy content of $600 \text{ MJ} = 166.65 \text{ kWh}$. For the same weight and energy content, the gasoline volume

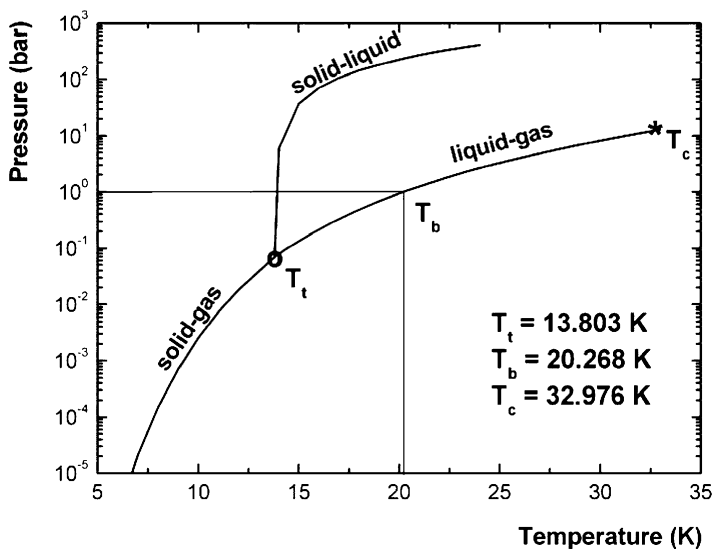


Fig. 3.1 Phase diagram of $p\text{-H}_2$. T_t represents the triple point ($T_t = -259.347^\circ\text{C}$, $P_t = 0.0704$ bar), T_b the boiling point ($T_b = -252.882^\circ\text{C}$, $P_b = 1$ bar), and T_c the critical point ($T_c = -240.174^\circ\text{C}$, $P_c = 12.928$ bar) [1]

is 0.019 m^3 . In view of these numbers, it is clear that for efficient storage, hydrogen density should be increased by reducing the volume taken by the gas under normal temperature and pressure conditions. As a consequence, the “usual state” of hydrogen has to be changed in order to store it efficiently. This can be accomplished by increasing the pressure, decreasing the temperature below the critical temperature or by reducing the repulsion interaction between hydrogen molecules by binding them with another material. Thus, the following three main options emerged:

1. Compressed hydrogen storage (CGH₂).
2. Cryogenic hydrogen storage (LH₂).
3. Solid storage of hydrogen (SSH₂).

The properties that are of importance in the use of hydrogen in the storage tank, in pipelines, and at the fuelling station are the flow of hydrogen, its composition, density, specific volume, specific heat,¹ conductivity,² viscosity, enthalpy, entropy, Joule–Thomson coefficient,³ and the velocity of sound in the gas.⁴

An outline of the requirements to guide current research and development and to achieve commercially viable hydrogen storage technologies is given by the U.S. DOE hydrogen storage system performance targets [2]. These targets are not based on a particular method or technology for storing hydrogen, but on equivalency to current gasoline storage systems in terms of weight, volume, cost, and other operating parameters. The ultimate goal is the implementation of hydrogen-powered fuel cell vehicles with a performance comparable or superior to today’s gasoline vehicles. Translating vehicle performance requirements into storage system’s needs resulted in the DOE hydrogen storage system targets. The storage system should include all the hardware (i.e. tank, valves, regulators, piping, mounting brackets, insulation, thermal management, and any other balance of plant components) in addition to the storage media and a full charge of hydrogen. Among others, the most important targets to be fulfilled by any storage system are the gravimetric and volumetric capacity, the refueling time (which depends on the thermodynamics of the materials and the thermal management for heat removal), and the minimum full flow rate.

Following a short description of the purification technology of hydrogen, this chapter will present various storage approaches that are currently of interest. They include the storage of hydrogen as compressed hydrogen gas (CGH₂) and cryogenic liquid hydrogen (LH₂). Then, solid storage (SSH₂) will be considered in the form of reversible and irreversible storage systems.

3.2 Purification of Hydrogen

The raw gas obtained by the methods described in Part I, Chapter 2 is delivered at various pressures and grades. Consequently, hydrogen has to be purified before compression, liquefaction or storage in a chemical form. The acceptable level of impurities for compression is around 4 ppm, whereas for liquefaction it should be below 1 ppm. This is to avoid any clogging of the different components in a liquefier (i.e. at 20 K, all the other elements except for He are solid).

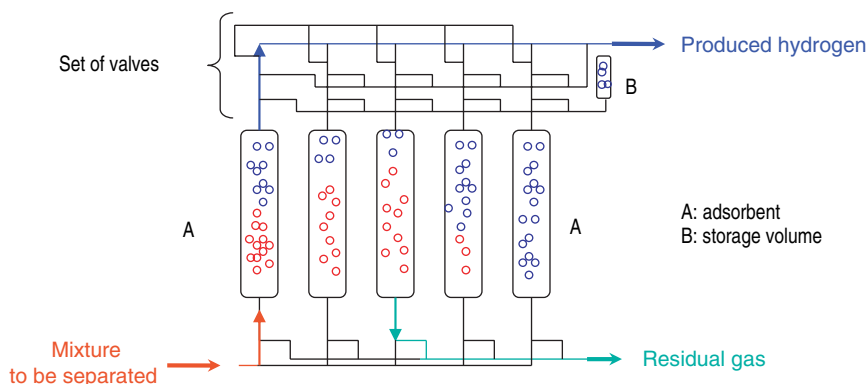


Fig. 3.2 Schematic diagram of a PSA unit with 5 adsorbents for hydrogen purification [3]

Purification of a gas can be performed by several techniques, such as separation by permeation, adsorption, absorption, distillation or by partial condensation [3]. For hydrogen the most common industrial technique is adsorption using a pressure-swing adsorption system (PSA) combined with or replaced by permeation or distillation processes. Figure 3.2 displays a typical system for hydrogen, which is composed of 5 adsorbents (the number of adsorbents actually depends on the extraction efficiency required), volumes for storage and for the stabilization of flow, and a set of valves. The process consists of feeding the raw gas under a certain pressure into the adsorbents (examples: Aluminates, silica gels, active charcoal, etc. in the form of stones, balls, sticks), where the heaviest constituents like CO_2 , H_2O , CH_4 , CO , Ar , and N_2 get captured while hydrogen passes through. The adsorbents are regenerated in several steps by decreasing the pressure and hydrogen reflux. At the outlet of this unit, hydrogen is purified to an impurity level of approximately 4 ppm. Further purification to an impurity level below 1 ppm is carried out using low-temperature adsorbents at liquid nitrogen temperature.

When hydrogen is produced by an electrolysis of water, traces of oxygen are removed in a “deoxo”, a reactor working at a temperature around 700 K with palladium as catalyst. Oxygen has to be removed not only to avoid the blocking of the piping and heat exchangers, but also for safety reasons to avoid the formation of an explosive mixture when the liquefier is warmed up.

3.3 Compressed Hydrogen (CGH_2)

3.3.1 Characteristics of CGH_2

Figure 3.3 displays the volumetric density of n- H_2 (normal hydrogen) as a function of the pressure at three different temperatures [1]. It can be seen that hydrogen density does not increase linearly with increasing pressure. A hydrogen density of

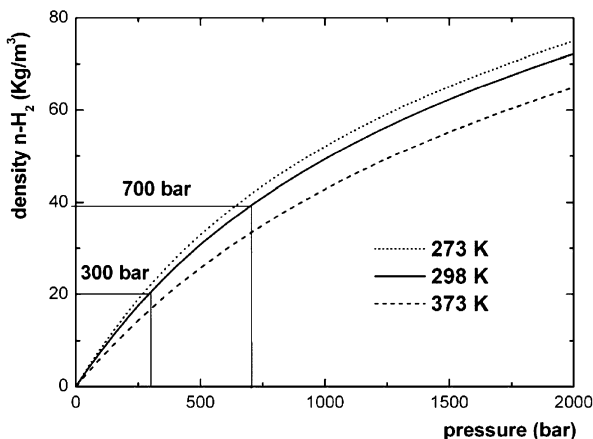


Fig. 3.3 Evolution of the volumetric density of n-H₂ as a function of pressure at three different temperatures [1]

20 Kg/m³ is reached at 300 bar. The volumetric density can be increased to around 40 up to 70 Kg/m³ by compressing the gas to a pressure of up to 700 or 2000 bar, respectively. However, 2000 bar is technically not feasible. Nowadays, a pressure of 350 bar is the standard and 700 bar is the current target value. High-pressure storage allows reducing the storage volume for 5 kg of hydrogen from 60 m³ to 0.25 and 0.125 m³ at a pressure of 1, 300, and 700 bar, respectively. The decrease of the storage volume from 300 to 700 bar is not as drastic as the decrease resulting when varying the pressure from 1 to 300 bar. Hence, another increase in internal pressure will not result in any significant breakthrough in volumetric density.

3.3.2 Hydrogen Compressors

A hydrogen compressor is a mechanical device that increases the pressure of the gas by reducing its volume. However, the low molar weight of hydrogen ($M = 2.016 \text{ g/mol}^{-1}$) requires the use of a volumetric compressor instead of a centrifugal compressor in order to gain efficiency. Moreover, the energy used to compress a gas does not only produce a pressure increase, but also generates heat. Compression work usually is calculated using the appropriate gas state and energy equations with two common approximations, adiabatic (isentropic) and isothermal compression.

In the adiabatic case, the process is assumed to take place without any heat exchange between the compressed gas and the environment and without variations of entropy. Under these conditions, the amount of work needed to raise the gas pressure from P_1 to P_2 ($P_1 < P_2$) is given by:

$$W_{\Delta S \rightarrow 0, ideal} = \frac{\gamma}{\gamma - 1} RT_1 \left[\left(\frac{P_2}{P_1} \right)^{\gamma/(\gamma-1)} - 1 \right] \quad (3.1)$$

where T_1 is the temperature of hydrogen at P_1 and γ is the specific heat ratio of the gas (C_p/C_v) that is assumed to be independent of temperature. For an adiabatic process, PV^γ is constant throughout compression. A correction factor, η_a is introduced to account for the irreversibility of an actual process.

For isothermal compression, the temperature of the gas is considered constant during the process. The compression work calculated under this assumption varies depending on whether ideal gas or real gas models are applied. The actual compression work will usually range between the theoretical conditions of isothermal and isentropic compression, which represent a lower and upper limit of compression work, respectively.

Generally, the compressed gas has to be cooled down after each stage to make compression less adiabatic and more isothermal. Hence, hydrogen typically is compressed in several stages. Important design parameters of a compressor are the inlet pressure and temperature, the discharge pressure, the required flow rate, the volume to fill, the start and end pressure, and the time allowed to fill the volume. Hydrogen compressors are expensive due to the materials used, their sizes, and their high maintenance costs of wear parts (e.g. valves, rider bands, piston rings). Moreover, compression is energy-intensive. At an inlet pressure of 20 bar and an outlet pressure of 70 bar with an adiabatic efficiency around 70 to 80%, for example, the compression energy required is between 0.6 and 0.7 kWh/kg. If the gas has to be compressed from 7 bar to 500 bar, the adiabatic efficiency is around 50 to 70% and compression energy is between 2.6 kWh/kg and 3.5 kWh/kg [4].

Types of compressors include mechanical piston and diaphragm compressors, non-mechanical compressors, such as the solid-state hydrogen compressor, and the electrochemical hydrogen compressor. Their properties and characteristics will be described shortly below.

3.3.2.1 Mechanical Compressors

These devices are used for filling vehicle tanks rapidly, moving gas between storage vessels, and unloading the gases from high-pressure tube trailers.

Piston Compressor

Figure 3.4 displays a single-stage piston compressor C12-40-7000LX/SS by Hydro-Pac, Inc. [5]. This compressor was designed for operation at a discharge pressure of 850 bar and inlet pressure of 350 bar. The capacity is around 430 kg/h at an inlet pressure of 350 bar and a motor size of 30 kW. Such a hydrogen gas compressor costs around US\$98,800 [5].

The piston compressor is an electro-hydraulically driven, non-lubricated, liquid-cooled, single-stage unit, including an electric motor, hydraulic pump, hydraulic oil reservoir, high-pressure gas intensifier, and intensifier shifting mechanism. The two major components are the intensifier and the fluid-power drive. As obvious from the

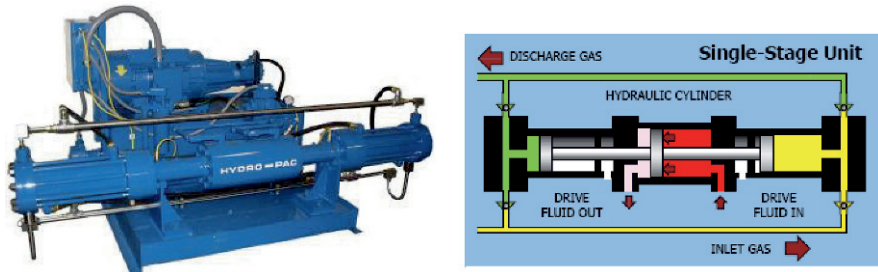


Fig. 3.4 Hydro-Pac hydrogen compressor model C12-40-7000LX for compression of hydrogen up to 80 MPa (800 bar), 30 kW (left). Single-stage unit with an inlet pressure of 35–40 MPa (350–400 bar) (right) [5]

schematic diagram of the single-stage unit, the intensifier contains a hydraulic drive cylinder in the center that is coupled by tie rods with two single-stage gas cylinders on either side. The fluid power drive provides the intensifier with pressurized hydraulic fluid. During operation, the gas fills the cylinder. Then, the force of the hydraulic pressure acts on the hydraulic piston compressing the gas in the first cylinder. Once compression is completed, the four-way valve redirects the hydraulic fluid and the piston assembly moves in the opposite direction. The special features of such a system are non-contamination of the compressed gas (using a non-lubricated design and isolated chamber for the fluid power and the compressed gas), the variable inlet pressure (using a high inlet pressure allows maximizing the compressor output), the near-isothermal compression due to the long, slow compression stroke (this allows reducing the power consumption), and reliability (the compressor has been used for thousands of hours in critical application).

Piston-metal Diaphragm Compressor

In this case, the gas from the piston and related components is isolated by a set of metal diaphragms as shown in Fig. 3.5 [6]. The piston moves a column of hydraulic fluid, which in turn moves the diaphragm set and displaces the gas to be compressed. As a consequence, the process is more isentropic than adiabatic, thus allowing to achieve a higher compression ratio. The deflection and inherent stresses of the metal diaphragms are controlled by a carefully designed cavity contour. This compressor compresses gases without any contamination of the process media or leakage of the gas into ambient air. Its service life is around 40,000 hours of continuous operation without any diaphragm or spare parts replacement. Under the EU project CUTE, three fully automated compressor systems were manufactured. This pilot compressor is self-contained and amenable to plug-and-play installation by the end user. Such a compressor has been installed in a wind park near Athens, Greece, Fig. 3.6, where hydrogen is produced by a water electrolyzer of 25 kW, which is supplied by a 500 kW gear-less, synchronous, multi-pole Enercon E40 wind turbine.

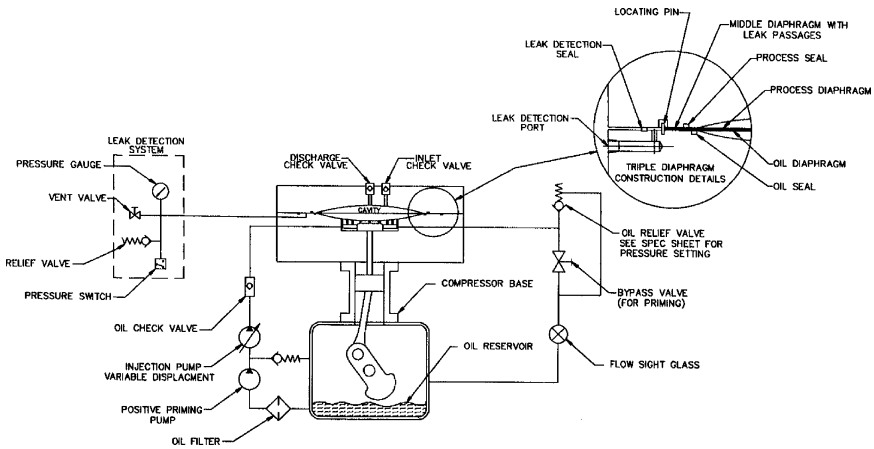


Fig. 3.5 Schematic diagram of a triple metal diaphragm compressor designed by PDC [6]

The compressor is used for filling high-pressure hydrogen cylinders. The compressor has a single-stage configuration with a maximum inlet pressure of 18 bar and a maximum outlet pressure of 400 bar and a flow of 5 Nm³/h. The compressor is powered by a 7.5 kW electric motor at 1450 rpm. The size is 1245 × 1014 × 1778 mm, total weight amounts to 907 kg. The compressor equipped with piping, accessories, instrumentations, heat exchangers, etc. costs around US\$60,000 [6].



Fig. 3.6 Wind farm near Athens, Greece, equipped with a PDC compressor [6]

3.3.2.2 Non-mechanical Compressor

These types of compressors have several advantages over mechanical hydrogen compressors, including smaller size, lower capital, operating, and maintenance costs, and the absence of moving parts, which eliminates problems related to wear, noise, and intensity of energy usage. Moreover, they can supply high-purity hydrogen.

Metal Hydride Compressor

The metal hydride compressors are thermally powered systems that use the properties of reversible metal hydride alloys to compress hydrogen without contamination. A wide range of pressures and pressure ratios can be obtained by selecting suitable alloys. The operating principle of the hydride compressor is based on heat and mass transfer in the reaction bed during absorption and desorption processes.

The selection of an adapted metal hydride alloy is important to reach the desired performance of the compression cycle. The thermodynamic (i.e. the enthalpy ΔH and the entropy ΔS obtained from the pressure-composition-temperature isotherm and the Van't Hoff plot), thermal (i.e. the specific heat C_p which controls the temperature increase produced by the addition of a given quantity of heat and the effective thermal conductivity λ which controls the diffusion of heat through the porous material), and kinetic (i.e. reaction rate which controls the flow of hydrogen) properties of the selected material should be characterized in detail in order to optimize compressor operation. Moreover, the materials should possess the properties listed below:

- Large hydrogen storage capacity.
- Good kinetic behavior for fast hydrogen flow from the compressor.
- High compression ratio in order to fill up a cylinder in a single-stage compression.
- Small hysteresis loss to ensure a high working compression ratio at convenient operating temperature.
- Good anti-poisoning and anti-aging characteristics.
- Wide and flat plateau pressures.

In addition, knowledge of metal hydride reactor heat and mass transfer characteristics is of importance for the design of hydride compressor. More details on the reactor design can be found elsewhere [7, 8, 9].

A single-stage thermal compressor is composed of a module filled with a reversible metal hydride alloy. Figure 3.7 displays the operation of the hydride compressor, which comprises four processes:

1. Hydrogen is absorbed into the alloy bed at low temperature (T_i) and at low pressure (P_i).
2. The module is subsequently heated from (T_i) to a higher temperature (T_f) with compression.
3. Compressed hydrogen is released at high temperature (T_f) and high pressure (P_f).
4. The module is cooled down from (T_f) to (T_i).

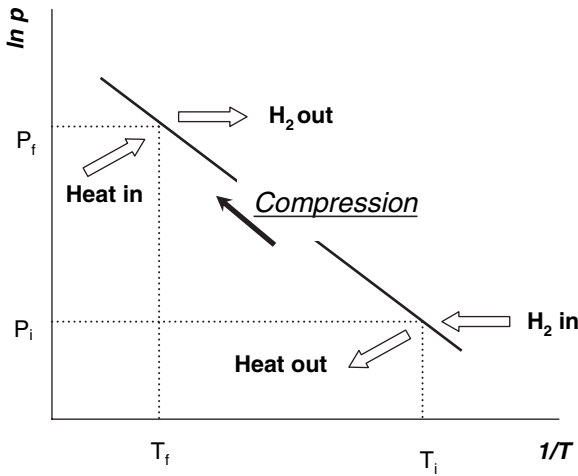


Fig. 3.7 Operation of a single-stage hydrogen compressor (Van't Hoff plot)

The pressure increases exponentially with increasing temperature. Hence, large pressure increases may be caused by moderate temperature increases only. An example is the $Mm_{1-x}Ca_xNi_{5-y}Al_y$ alloy (where Mm is mixed metal) which takes up industrial hydrogen at 2 MPa (20 bar) and 20°C and gives ultra-pure hydrogen at 10 MPa (100 bar) and 95°C with hot water only being used as a source of heat [10].

To obtain higher pressures, a multi-stage thermal compressor is used, which consists of several modules connected in series. Each module contains a different metal hydride alloy and hydrogen is successively absorbed into and desorbed out of several hydride beds [9, 11]. The driving force exerted by a variation in temperature and the difference of enthalpy between alloys of the coupled module gradually increases the exit pressure from one stage to the next one. An example is the double-stage compressor in which an AB_5 type alloy is used as the low-pressure stage alloy and an AB_2 as the high-pressure alloy to compress industrial grade hydrogen at a pressure of around 2 MPa to ultra-pure hydrogen with a pressure of up to 45 MPa [9]. Figure 3.8 displays the thermodynamic principle of the above double-stage compressor. The Van't Hoff plots corresponding to the absorption and desorption of the two alloys are represented. Point 1 represents the absorption of hydrogen by the AB_5 alloy and the removal of the heat produced by cool water. Then, the hydride bed is heated with 99°C hot water and hydrogen at a pressure around 10.5 MPa is produced, as indicated by point 2. This hydrogen is subsequently fed into the high-pressure-stage compressor (point 3), which is cooled by 20°C water. The AB_2 alloy absorbs hydrogen rapidly due to the fact that the pressure from the low-compressor stage is higher than the hydriding plateau pressure of the AB_2 alloy. This hydride bed is heated with 99°C hot water and high-purity hydrogen at 45 MPa is released (point 4).

The metal hydride compressor operates by cycling between two temperatures. Therefore, its energy needs mainly consist in heating and cooling resources. Hot

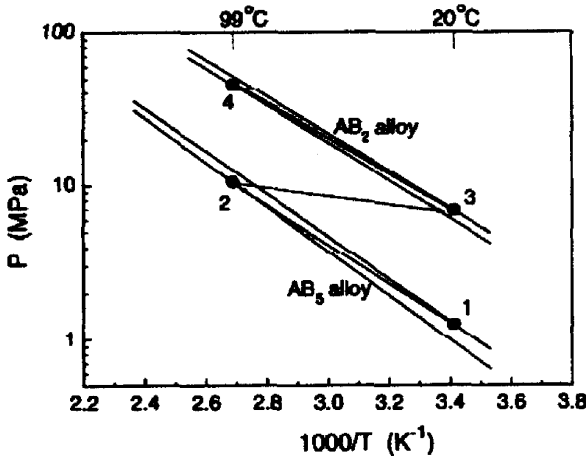


Fig. 3.8 Thermodynamic principle of a double-stage hydrogen compressor [9]

fluids or electric heating of the beds may provide for the compression energy. Thermal compression is not based on the adiabatic process and thermal efficiency can be calculated as follows:

$$\eta = \frac{W}{Q} = \frac{W}{Q_1 + Q_2} \quad (3.2)$$

where $W = f(P_{eq})$ is the compression work from T_i to T_f . The equilibrium pressure is estimated by the Van't Hoff equation as

$$\ln P_{eq} = \frac{\Delta S}{R} - \frac{\Delta H}{RT} + f_{\text{hysteresis}} + f_{\text{slope}} \quad (3.3)$$

Q in Eq. (3.2) represents the total energy used to compress n mol of hydrogen. Q_1 is the energy used to heat the hydride from T_i to T_f and Q_2 the thermal energy that makes the hydride release hydrogen. For a double-stage compressor $Q_1 = [(m_I C_{pI} + m_{II} C_{pII})(T_f - T_i)]$, where m and C_p are the weight and the specific heat of the hydrogen storage alloys I and II, respectively, and $Q_2 = [n(\Delta H_I + \Delta H_{II})]$, where n is the molar number of compressed hydrogen.

Electrochemical Compressor

This type of compressor is used when a small quantity of hydrogen has to be compressed to high pressure, because it is more efficient than the mechanical compressor in this regime [12]. The working principle is based on an electrochemical cell, Fig. 3.9, composed of an anode, a membrane electrode assembly (MEA), and a cathode [13]. When a potential difference is applied, the hydrogen at a pressure P_a is oxidized to H^+ at the anode. These ions are transported through the membrane to the cathode, where they are reduced to hydrogen at a pressure $P_c > P_a$, if the cathode

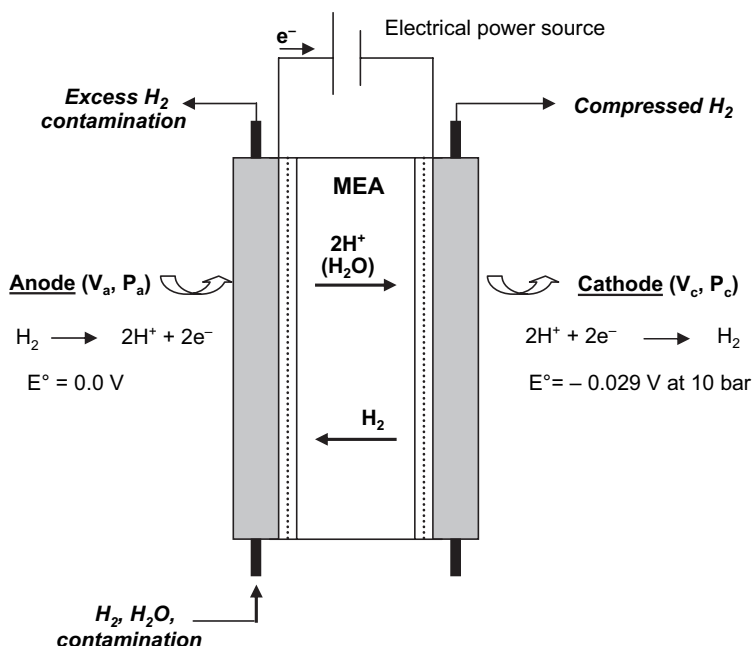


Fig. 3.9 Principle of the electrochemical hydrogen compressor [13]

compartment is hermetically sealed. A multi-stage electrochemical hydrogen compressor incorporates a series of membrane electrode assemblies (MEAs). It should be noted that the process is selective for hydrogen, as the inert gas components cannot pass the membrane.

With an electrochemical compressor, hydrogen can be compressed from ambient pressure to 16 MPa for example [14]. A main parameter that affects the efficiency of such a compressor is the humidification of the membrane. In fact, the membrane has to be saturated with water to have a good ionic conductivity (i.e. protons are only transported, if they cross the membrane in the hydrated form). Therefore, diffusion studies are carried out using different membranes to determine the relationship between membrane thickness and diffusion rate [13]. Research relating to membrane materials which can work as a proton conductor without any further humidification at ambient temperature has shown that a single MEA film of hydrogen sulfated fullerene [C₆₀(OSO₃H)_n(OH)_n] can be used to compress hydrogen up to 1 MPa [15].

3.3.3 Storage of CGH₂

Once hydrogen is compressed, the next important factor for application is to have a high volume of hydrogen carried per unit weight of the container. Consequently,

use of such a high pressure of hydrogen implies an appropriate ultra-lightweight material for the construction of the storage cylinders and the compressors, which can withstand the applied pressure and resist the effects of hydrogen embrittlement⁵ and has a low hydrogen permeability. Progress achieved in both the materials of construction and manufacturing technology increased the technical efficiency of the cylinders from 0.05 m³/kg (500 kg vessel made of wrought iron for a gas capacity of 25 m³) in 1880 to around 0.13 m³/kg (low-alloy steels with the addition of 1% Cr and 0.2% Mo) in the mid-1960s [16]. Nowadays, technical efficiency is 0.70 m³/kg for a 110 kg vessel made of three layers of composite materials. Gas capacity amounts to 77 m³ [16]. The state of the art of current compressed gas tanks, including design requirements and safety features, is described in more detail in Part II, Chap. 8a by Sirosh and Niedzwiecki from Quantum Technologies Inc. [17].

3.3.4 Outlook

Storage of hydrogen as a compressed gas is close to technical feasibility. Compressed storage is of interest to small city cars and large vehicles. The major difficulty is the volume needed to store the hydrogen and the energy required for the compression of the gas. Therefore, research is going on to improve the storage cylinders by optimizing materials and to develop design principles and an efficient method to compress hydrogen. In addition, special seals and/or tolerance standards are investigated to achieve high pressures. New approaches, including guided rotor compressors and linear compressors, are pursued. At the moment, the critical issue for an accelerated market penetration is the cost of hydrogen compression and storage cylinders.

3.4 Liquid Hydrogen (LH₂)

A second method to increase the density of hydrogen is to decrease the temperature of the gas at a constant pressure to obtain the liquid phase. The normal hydrogen, n-H₂, which corresponds to the equilibrium mixture at room temperature, is a gas composed of 75% o-H₂ (ortho-hydrogen) and 25% p-H₂ (para-hydrogen). The ortho- and para-hydrogen are the two isometric forms of the hydrogen molecule depending on the relative orientation of the nuclear spin of the individual atoms [1]. The molecules with a parallel nuclear spin, called ortho-hydrogen, o-H₂, are on a higher energy level than the molecules with an anti-parallel nuclear spin, called para-hydrogen, p-H₂ (stable state). The percentage of ortho–para concentrations in the mixture at equilibrium is temperature-dependent as displayed in Fig. 3.10. When the temperature decreases, a conversion takes place slowly to 100% p-H₂, which is the stable phase at 20 K. The conversion reaction from the n-H₂ to the p-H₂ state is a reversible and exothermic reaction that occurs without breaking the H–H bond.

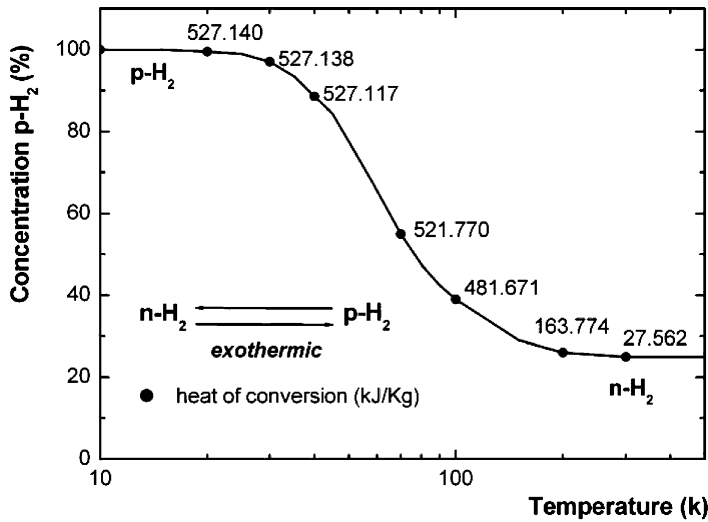


Fig. 3.10 Evolution of the concentration of p-H₂ at equilibrium as a function of the temperature. The heat of conversion is given in kJ/kg [1]

3.4.1 Characteristics of Liquid Hydrogen

As shown in Fig. 3.11, the density of liquid hydrogen is around 80 kg/m³ at 22 K and a pressure of 4 bar. Hence, liquid hydrogen needs less storage volume than the gas (one liquid hydrogen container can substitute approximately 7 to 8 CGH₂ trailers). That is why liquid hydrogen is of interest, although the unusual properties of hydrogen described below impose several technological constraints to the liquefaction process and cryogenic storage.

The boiling temperature of hydrogen is 20 K at 1 bar. At this temperature, natural gas and other gases are solid. Consequently, hydrogen should be purified to a level below 1 ppm before its liquefaction in order to avoid any clogging of the heat exchangers, which in turn will decrease the overall efficiency of the liquefier.

Hydrogen has a peculiar Joule–Thomson effect inversion temperature of around 190 K at a pressure below 50 bar. As a consequence, a process other than a Joule–Thomson expansion has to be used to cool hydrogen from 300 to 190 K.

The vaporization enthalpy of hydrogen is very low. Hence, an excellent thermal insulation is required in the coldest part of the liquefier as well as in the storage vessel to minimize the loss by vaporization.

The molar weight of hydrogen is 2.016 g/mol, which is 14 times less than that of nitrogen. Consequently, the kinetic energy of hydrogen at a certain pressure and temperature is 14 times smaller than that of nitrogen. Hence, use of the volumetric piston compressor is recommended instead of a centrifugal compressor.

The conversion from n-H₂ to p-H₂ is naturally a slow and exothermic reaction, where the heat of conversion is temperature-dependent as can be seen in Fig. 3.10. It

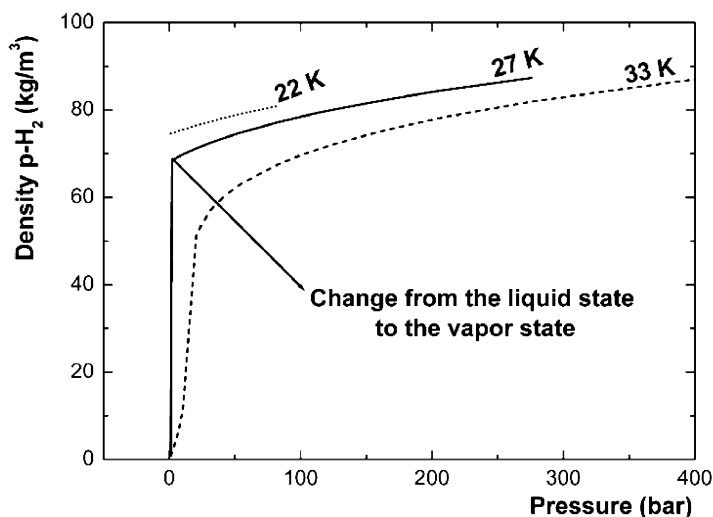


Fig. 3.11 Evolution of the density of liquid hydrogen as a function of pressure at three different temperatures

increases non-linearly when the temperature decreases, from 27.562 kJ/kg at 300 K to 527.140 kJ/kg at 20 K [18]. At 20 K, the heat of conversion from n-H₂ to p-H₂ (around 527 kJ/kg) is higher than the heat of vaporization of n-H₂ (454 kJ/kg). This implies that the reaction has to be accelerated and cooled in order to minimize the reversibility of the reaction. Therefore, exothermic conversion takes place with a catalyst and the most common one is iron oxide Fe(OH)₃ obtained from the reaction of NaOH with FeCl₃. The exothermic catalytic conversion may be of adiabatic, isothermal or continuous type [19].

- In the *adiabatic conversion* the catalyst is installed in a container, where the hydrogen is flowing. As a consequence, the hydrogen temperature increases during the conversion and it has to be cooled down again.
- In the *isothermal conversion* the catalyst is installed in a container maintained at a constant temperature by a cryogenic liquid at its boiling temperature. The heat released during the conversion of hydrogen then vaporizes the cryogenic liquid.
- In the *continuous conversion* the catalyst is integrated in the heat exchanger, where the hydrogen is flowing. This allows for a constant removal of the conversion heat released. Thus, the hydrogen remains close to the ortho–para equilibrium at every temperature.

Each of these modes can be integrated in the design of a liquefier. However, the continuous conversion mode has the best efficiency.

The liquefaction cycles are based on two thermodynamic expansion processes:

1. Isenthalpic expansion or Joule–Thomson expansion which is performed using a valve.

2. Imperfect isentropic expansion or an expansion with energy extraction using an expansion turbine or an expander. In this case, no liquid is formed at the end of the expansion.

Perfect adiabatic conditions are not feasible in an LH₂ storage reservoir, implying that losses due to heat flux can only be minimized, but not avoided.

3.4.2 Liquefaction of Hydrogen

Dewar (British) was the first to realize the liquefaction of hydrogen in 1898. Subsequently, Prof. Linde (German) conceived the first liquefier by compression in 1900. Later, Claude (French), founder of Air Liquide, improved this machine.

Hydrogen gas has to be cooled down from 300 to 20 K taking into account its particular physical properties, such as the low boiling temperature, the low Joule–Thomson effect inversion temperature, the slow exothermic ortho–para conversion, the large variation of heat conversion with temperature, and the internal heat leaks. As a consequence, the design of an efficient liquefier (i.e. high product yield with low energy cost) depends on the selection of an optimized liquefaction cycle and equipment.

3.4.2.1 Design of a Liquefier

The liquefaction process of hydrogen combines the effect of cooling with an adiabatic expansion of the gas. The hydrogen gas should be purified first to an impurity level below 1 ppm and compressed to 20 bar (as the optimum pressure to liquefy hydrogen is above the critical pressure), before it is delivered to the inlet of the liquefier. The main components of a liquefier are:

- Compressors.
- Heat exchangers.
- Turbines to decrease the temperature of hydrogen and to extract some energy that would be lost.
- Expanders to provide cooling at various points of the cycle.
- Intercoolers to remove the heat between the different stages of compression.
- Pumped liquid nitrogen or hydrogen bath to supply extra cooling to the heat exchangers.
- A Joule–Thomson expansion valve to produce some liquid.

All cryogenic equipment should be enclosed by a single cold box with a vacuum and multi-layer insulation in order to minimize evaporation loss. Moreover, most of these components are made of high-strength materials, such as Cr and Mo steel, in order to withstand the low operating temperatures and resist hydrogen embrittlement and permeability.

The simple liquefaction system is based on a pre-cooling of the gas using a nitrogen cycle (from 300 to 80 K) in series with an ortho–para converter (from 80 to 30 K) and a Joule–Thomson valve for expanding the gas at 20 K to produce liquid hydrogen.

An optimization of the liquefier, known as a Claude cycle, is obtained by separating the cooled gas from the liquid and returning it to a 2-(or 3, 4)stage compressor via the heat exchanger [19]. A schematic diagram based on a two-stage compressor Claude system is displayed in Fig. 3.12. The cycle comprises the main line to liquefy hydrogen as described above and two compressors in series. The first compressor pressurizes the return gas from Joule–Thomson expansion and the vapors generated by the storage of liquid hydrogen. The second one compresses to a pressure of 50 bar the outlet gas from the first one and the flux from the expansion turbines.

The efficiency of the liquefier η is the ratio between the theoretical work W_{th} required and the real work W_r . The theoretical work includes the energy necessary to cool hydrogen from ambient temperature to 20 K, the heat due to the phase transformation, and the heat of conversion from n-H₂ to p-H₂. The ideal work for the liquefaction of hydrogen from 300 K at 1 bar to 20 K at 1 bar is equal to an electric energy requirement of 3.9 kWh/kg. This energy is decreased to 2.8 kWh/kg, if the feed hydrogen gas is compressed to a pressure of 30 bar. In addition, the real work

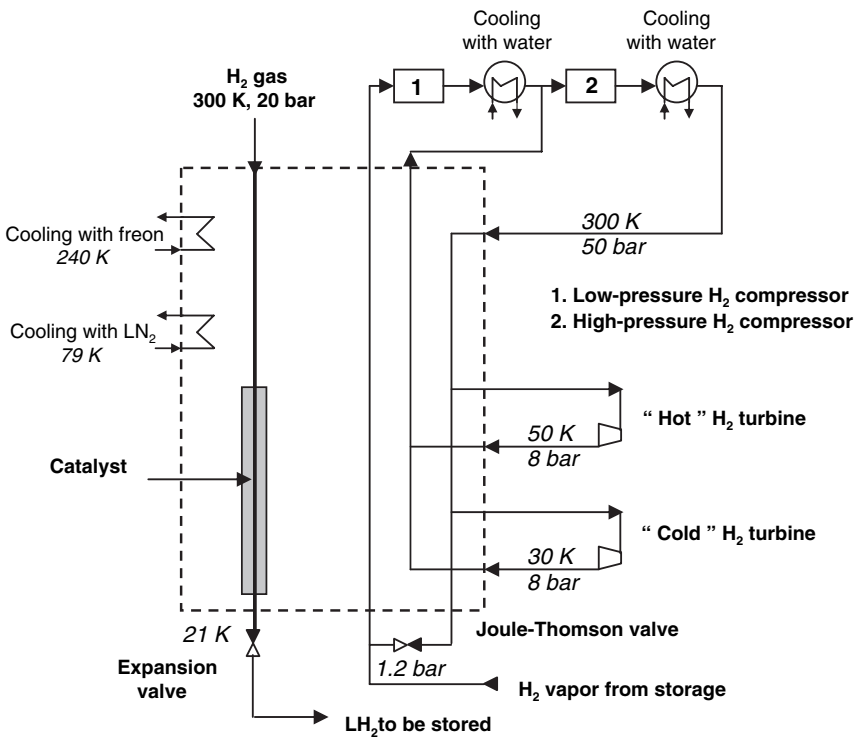


Fig. 3.12 Schematic diagram of hydrogen refrigeration based on the Claude cycle [19]

depends on the thermal insulation of the liquefier, the efficiency of the heat exchangers, and the compressors. Hence, the efficiency of a liquefaction plant increases with its size and, hence, production rate.

3.4.2.2 Industrial Liquefiers

Large-scale hydrogen liquefaction plants are based on the Claude cycle, where hydrogen is used as the refrigerant. Existing plants differ in design by the number of turbines and compressors used as well as by the type of converter used to carry out the exothermic conversion. Ten hydrogen liquefaction plants are located in North America with a capacity ranging from 5.4 tons/day to 32 tons/day [3]. There are only three hydrogen liquefaction plants in Europe. Air Liquide owns and operates one liquefier in Waziers, France. The second one is operated by Air Products in Rozenburg, Netherlands, and the third one by Linde in Ingolstadt, Germany. The hydrogen liquefaction capacities of the three liquefiers are 10.5, 5.4, and 4.4 tons/day, respectively. Total capacity in Europe presently is 20 tons/day equivalent to 230,000 Nm³/day or 84 million Nm³/year. In addition, Linde will build another liquefier which will have a daily tonnage of 5.7 tons in Leuna. The industrial liquefiers by Linde and Air Liquide will be described briefly below.

Liquefier by Linde

The hydrogen liquefier in Ingolstadt (Germany) designed by Linde is located on the site of a refinery which supplies hydrogen-rich raw gas (H₂ concentration is around 86%) [20]. Figure 3.13 displays the schematic diagram of the liquefaction process. The raw gas is supplied at around 3300 Nm³/h, with the pressure varying between 9 and 14 bar. The raw gas is first compressed to 20 bar and then purified in a pressure-swing adsorption system to an impurity level of about 4 ppm. After purification, the hydrogen can be passed to the high-pressure line (where it is compressed to 225 bar using a piston compressor) or the liquefaction line.

The liquefaction line is designed for a capacity of 2000 Nm³/h and based on a Claude cycle. The liquefier is composed of one adsorber, six plate-type heat exchangers, two ortho/para Fe(OH)₃ catalysts outside of the heat exchanger, one LN₂ bath with catalyst, one LH₂ bath with catalyst, three expansion turbines, two Joule–Thomson valves, and two compressors. All cryogenic equipment is enclosed in a single cold box. Prior to refrigeration, the hydrogen is first purified to an impurity level below 1 ppm using a low-temperature adsorber. Then, three temperature levels are applied:

1. Up to 80 K using liquid nitrogen.
2. From 80 to 30 K using expansion turbines.
3. From 30 to 20 K using Joule–Thomson expansion valves.

Ortho/para hydrogen conversion is accomplished using two adiabatic converters and two isothermal converters with liquid nitrogen and hydrogen baths. Moreover, work is extracted from the cycle gas by three expansion turbines arranged in series.

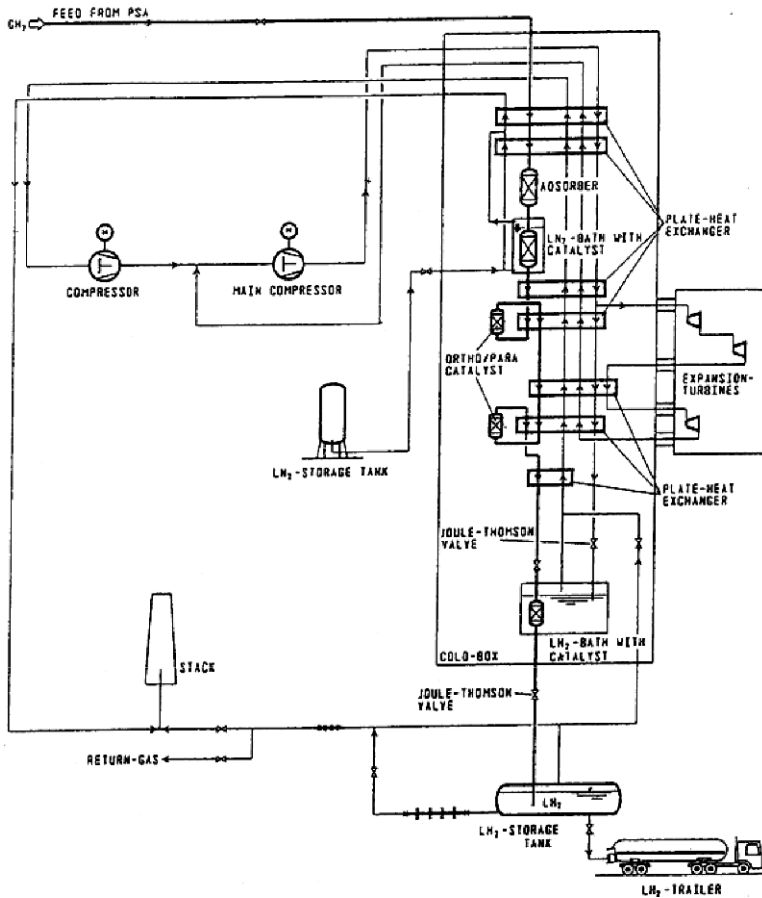


Fig. 3.13 Schematic diagram of the hydrogen liquefier by Linde [20]

The daily output is 4.4 tons and the produced LH₂ is stored in a vacuum-insulated 270 m³ tank with a loss of 0.3% per day. Considering the whole liquefaction process and taking into account a specific production energy of 0.4 kW/h for the liquid nitrogen, the specific energy per liter LH₂ is 0.9 kWh, which corresponds to a thermodynamic efficiency of about 33% of that of an ideal Carnot cycle with four-stage ortho–para conversion.

Liquefier by Air Liquide

Air Liquide owns one hydrogen liquefier cycle in Kourou for the rocket test facilities ARIANE IV and V [19]. This liquefier uses hydrogen produced by catalytic reforming of methanol at 600 K according to the following reaction:



The hydrogen produced is first purified to an impurity level below 1 ppm. Then, it is cooled and liquefied in three steps as follows:

1. From 300 to 230 K using mechanical refrigeration.
2. From 230 to 80 K using a nitrogen cycle.
3. From 80 to 20 K using a hydrogen cycle.

The nitrogen cycle comprises one N_2 compressor and a N_2 turbine. The hydrogen cycle is composed of two H_2 compressors in series and two H_2 turbines. Heat exchange between 300 and 20 K is performed in vacuum-brazed aluminum plate fin exchangers. Exothermic catalytic conversion is performed by continuous conversion. All pieces of cryogenic equipment are enclosed in a single cold box with vacuum and multi-layer insulation.

The liquefaction capacity is 2.3 tons per day and the liquid hydrogen is stored in several reservoirs of 323 m^3 with a daily loss of less than 0.3%. The efficiency of the liquefier is around 40%.

3.4.3 Liquid Hydrogen Storage

The liquid hydrogen supplied by the liquefier has a high purity and high storage density. Typically, the LH_2 is stored in a dual-walled stainless steel vessel with vacuum super-insulation between the inner and the outer vessel consisting of several highly reflective radiation shields separated by an appropriate spacer material in order to minimize losses due to radiation, convection, and conduction heat, as perfect adiabatic conditions are not feasible [21, 22]. The storage tank will always have intrinsic heat leaks which can be minimized, but not avoided. As a consequence, hydrogen always evaporates after filling the tank. Thus, the ratio between liquid and gas (part of the liquid evaporates to gas) changes and this leads to a pressure increase. From a certain pressure, gas is released. From this point, the temperature inside stays the same until all the gas has evaporated. These heat leaks only depend on the temperature difference between the inside and outside of the vessel. They are an intrinsic feature of the vessel and depend on the quality, capacity, and the shape of the tank only.

Evaporation rate is proportional to the surface to volume ratio and a linear function of the total heat flux. Therefore, evaporation losses can be decreased by increasing the volume of the tank (the best shape actually is a sphere). Losses are in the order of 0.3% per day for a vacuum-insulated 320 m^3 tank, whereas they amount to 5% per day for a 102 l cryogenic vehicular tank with a total heat entry of 1.7 W. A more detailed description of the cryogenic tank, from the requirements to the design in mobile application, can be found in Part II, Chap. 8b by Michel from Air Liquide.

3.4.4 Liquefaction Cost

The total investment costs (i.e. building construction cost, components cost, engineering, overhead and administration, start-up expenses, etc.) of a liquefaction plant

with a capacity of 150 tons/day, for example, is around US\$200,000,000 [23]. The liquefaction process is very energy-intensive, as typical unit powers are in the order of 12.5 to 15 kWh/kg. The liquefaction costs of a large-scale liquid hydrogen plant primarily depend on the energy costs

The liquefaction of hydrogen gas needs energy which cannot or only partly be re-covered in the re-vaporization process. Hence, liquefaction energy is a loss of the overall system and it should be minimized. The prime cost factor for large systems is power consumption which is related to the basic efficiency of the selected cycle and the efficiency of the different components like compressors, heat exchangers, and expanders. Energy analysis indicates that the higher the hydrogen is compressed at ambient temperature, the lower is the power needed for the cooling from 80 to 30 K. In addition, conversion should take place in the continuous mode in order to have the smallest irreversibility. The compressor is the most important part with respect to both cost and its ability to influence the overall performance of the system [24]. It was demonstrated that several stages of compression with intermediate cooling are required to minimize the power consumption. Another component of importance is the heat exchanger which should be compact with a counterflow configuration and an operating pressure around 25 bar [24].

An innovative conceptual design of a large-capacity hydrogen liquefier proposed by Quack indicates that a thermodynamic efficiency in the order of 60% can be reached with a power requirement of 7 kWh/kg [25]. The proposed liquefier is designed in the following way:

- Hydrogen gas is compressed from 1 to 80 bar in 5 stages with a pressure ratio per stage of about 2.4. The overall power consumption can be reduced by using intercoolers cooled with water in the first stage and a propane refrigerator.
- The ortho-para conversion is carried out in the continuous equilibrium mode with two main heat exchangers.
- Cooling from 300 to 73 K is proposed to be performed with a helium/neon mixture as refrigerant instead of the “classical” nitrogen cycle.
- Cooling from 73 to 25 K is performed with a helium-neon cycle using 6 expanders.
- Cooling from 25 K to storage conditions is carried out by expansion of the hydrogen stream from 80 to 1 bar. The flash gas is compressed by a cold compressor to a pressure level, where it can be condensed by the helium cycle. At the outlet of this condenser, a simple throttling process is used to obtain the saturated liquid at 1 bar.

It should be noted that if the pressure of the feed hydrogen is around 20 bar instead of 1 bar as selected in this design with a storage pressure of 3 bar, the total power requirement of the liquefier would decrease to around 5 kWh/kg.

To summarize, large-scale plants have to be built to decrease capital cost. Further research is needed with respect to new compression and expansion technologies with high-speed centrifugal compressors with titanium wheels as proposed by Quack and possibly expanders to decrease energy consumption [25]. Materials development is required to lower the cost of the high-efficiency insulation of

the storage vessels. New approaches to low-temperature refrigeration, which are still in the research and development stage, include cooling by magnetic refrigeration. The active magnetic refrigeration (AMR) is based on the magneto-caloric effect of the materials used close to their transition temperature. This means that the absorption and release of the heat occur by the change of temperature due to the adiabatic magnetization/demagnetization of the material [26, 27, 28, 29, 30, 31]. The main advantage of this process is that the energy loss is close to zero during the adiabatic magnetization/demagnetization cycles compared to the classical compression/expansion process.

3.4.5 Outlook

Cryogenic liquid hydrogen has a much higher volumetric density than gaseous hydrogen, resulting in lower transport and storage costs. Nowadays, liquefaction technology is safe, reliable, and produces daily tonnage quantities. However, for the use of liquid hydrogen on a large scale, an increase in liquefier efficiency is required to reduce energy costs, since current liquefaction technology is costly and presently consumes more than 30% of the stored energy. This implies an optimization of liquefaction cycles and equipment to produce large volumes of liquid hydrogen with low energy requirements. Components subject to optimization include compressors, turbine expanders, and heat exchangers.

Moreover, research relating to lightweight materials for the tanks and the reduction of the daily loss due to thermal heat needs to be continued. Current research also focuses on active or passive cooling systems to increase the stand-by time before evaporation losses occur.

3.5 Solid Storage of Hydrogen (SSH₂)

Hydrogen stored in a solid-state material has potential advantages compared to compressed or liquid hydrogen storage in terms of volumetric density (it requires one third of the volume of a pressurized hydrogen gas tank at 345 bar) and safety (heat is required to deliver hydrogen), technology, and available resources.

The parameters which are of importance to hydrogen storage are the gravimetric and volumetric densities on the system basis. Furthermore, hydrogen uptake and release should be reversible. Finally, the net energy has to be taken into account. This includes the energy needed to manufacture the storage system, to produce and to store it. The technical requirement defined for a standard car is that 5 kg of hydrogen shall be stored to have a range of 500 km. This means that only hydrides with the highest possible gravimetric hydrogen storage capacities are viable for potential commercial automotive application. Moreover, the temperature and pressure during

operation shall be in the range from 20 to 358 K and 0 to 6 bar, respectively, in order to match the operating conditions of the fuel cell. Other important requirements are:

- A relatively low desorption temperature compatible with a PEM fuel cell.
- Relatively fast kinetics of hydrogen desorption.
- The filling time should not exceed 5 minutes.
- Cycling stability.
- Low density of hydride.
- Low hydride price.

Although huge numbers of compounds were investigated in the last years, no system has been found so far that would be able to fulfill all requirements. Hence, new approaches had to be pursued. One is to modify the properties of the known materials by atomic substitution, addition of dopants, by using nanoscale materials instead of bulk material (as nanostructurization was found to improve the kinetic properties of the material), etc.

Current research focuses on reaching the volumetric and gravimetric capacity targets, meeting the energy and temperature requirements for hydrogen release, fulfilling the appropriate charging and discharging rate of hydrogen (i.e. good kinetics), and understanding the fundamental mechanism of the hydrogenation/dehydrogenation reaction. The materials investigated may be divided into reversible and irreversible storage systems. Both of them may be considered on-board storage systems. The difference is that the irreversible system is regenerated off-board.

3.5.1 Reversible Storage Systems

Reversible storage system means that the material may be refilled, recharged with gaseous hydrogen on-board the vehicle. In practice, two basic mechanisms may be considered for hydrogen storage:

1. Physisorption which implies the adsorption of molecular hydrogen by the material.
2. Chemisorption which implies the dissociation of hydrogen molecules and subsequent chemical bonding of H atoms by integration in the lattice of a metal, alloy or by formation of a new chemical compound.

In the following sections, selected compounds will be presented for these two approaches, which are of interest for hydrogen storage in solid-state materials.

3.5.1.1 Hydrogen Storage by Physisorption

Physical adsorption is based on weak Van der Waals forces between the adsorbate molecules and the adsorbent. The interaction energy for molecular hydrogen

typically is between 1 and 10 kJ/mol. The order of magnitude of the interaction depends on the nature of the gas molecule and on the adsorbing material.

As a consequence of the low adsorption energy involved in the physisorption process, physical adsorption is completely reversible and fast refueling is possible without the problem of heat management. However, higher hydrogen storage capacities can be obtained at lower temperature only, typically at 77 K. Different classes of materials, such as active charcoal, nanostructured carbon [32, 33, 34, 35], zeolites [33, 36], and metal organic framework [37, 38, 39, 40, 41], have been investigated for hydrogen storage by adsorption at low temperature. Among the examples presented below are carbon nanostructures and the metal organic framework, as they are the most promising systems.

Nanostructured Carbon

A great variety of carbon nanostructures exists, such as activated carbon, carbon nanofibers, multi-walled carbon nanotubes (MWCNT) and single-walled carbon nanotubes (SWCNT), carbon nanohorns, etc. They all consist of benzene-like carbon hexagons with sp^2 -hybridized carbon atoms, but they differ from each other in the way these hexagons are arranged in the material. By different synthetic procedures and treatments of carbon materials, it is possible to design a nanostructure with the desired surface area and pore density.

The hydrogen storage capacity is measured volumetrically with a Sievert's type apparatus at room temperature (RT) and 77 K. Figure 3.14 displays the kinetics of hydrogen uptake at 77 K and at RT. At 77 K, a type I adsorption isotherm (or Langmuir isotherm), characteristic of microporous solids is observed [35]. The isotherm exhibits two regions with an increase in hydrogen uptake at low pressure followed by a horizontal plateau at high pressure. The initial increase depends on the heat of

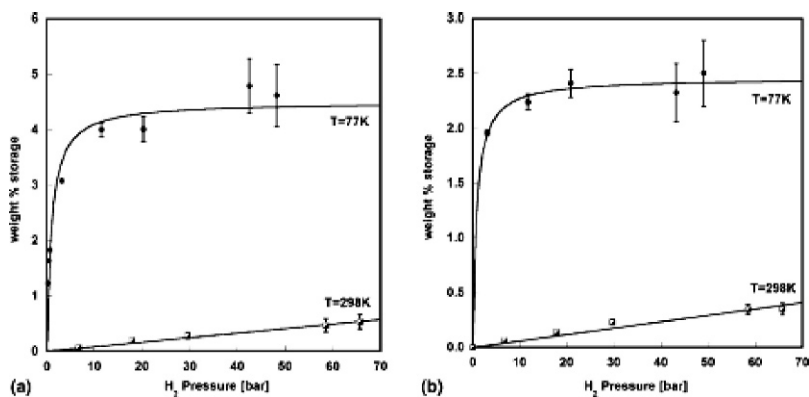


Fig. 3.14 Hydrogen adsorption isotherms at room temperature and at 77 K fitted with a Henry type and a Langmuir type equation, respectively, (a) for activated carbon, (b) for purified SWCNTs [35]

adsorption, while the plateau is independent of the interaction energy and reflects the complete coverage of the adsorbent's surface. At RT, a linear Henry type isotherm is observed. The storage capacity is very low, indicating that only a fractional coverage takes place with the formation of a highly diluted monolayer.

The hydrogen storage capacity is based on the local interaction between hydrogen molecules. It has been shown that the hydrogen storage capacity almost is a linear function of the specific surface area at room and at low temperature [33, 35]. By developing microporous materials with a large specific surface area, it is therefore possible to increase the storage capacity. Moreover, it has been demonstrated that a correlation exists between the microporous volume and the adsorption storage capacity [35, 42, 43]. To identify the whole microporosity range, carbon materials are characterized by N_2 adsorption isotherms at 77 K to determine the total volume of micropores smaller than 2 nm in size and by CO_2 adsorption at 273 K for micropores smaller than 0.7 nm in size. The linear relation found between the hydrogen adsorption capacity and CO_2 micropore volume suggests that the presence of a homogeneous narrow microporosity (≤ 0.7 nm) is of importance to hydrogen adsorption [35, 42]. Hence, carbon materials ideal for hydrogen storage should possess a high specific surface area as well as a high microporosity with a small pore dimension.

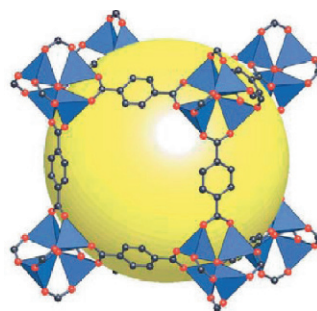
However, the amount of hydrogen adsorbed by the best carbon material (labeled Activated Carbon I, obtained from the reaction of coke with KOH) with an SSA of $2564 \text{ m}^2/\text{g}$, an average pore diameter of 1.18 nm, and a pore volume of $0.75 \text{ cm}^3/\text{g}$ for pores with a radius less than 0.65 nm is limited to 0.54 wt.% H_2 at 298 K and 65 bar of hydrogen and to 4.4 wt.% at saturation and 77 K [35, 36].

Metal Organic Framework (MOF)

Metal organic frameworks with an SSA between 2500 and $4000 \text{ m}^2/\text{g}$ are a new class of microporous materials which reach the highest theoretical SSA value for carbon material of about $2600 \text{ m}^2/\text{g}$. These materials are composed of metal oxide groups connected to each other by a rigid structure. They are the lightest known crystalline materials with densities down to $0.21 \text{ g}/\text{cm}^3$. These materials allow for the design of a network with the metal centers and pore dimensions desired.

To date, hundreds of different MOFs have been synthesized with a great variety of network topologies [37, 38, 39]. The most famous porous structure is MOF-5 [37, 38] displayed in Fig. 3.15. It consists of Zn_4O clusters at the corners of a cube and connected to each other with benzene-1,4-dicarboxylate $O_2C-C_6H_4-CO_2$ as ligand to give an extended 3D cubic framework and, hence, a crystalline solid with interconnected pores of 0.8 nm aperture width and 1.2 nm pore diameter. Different metal centers like Mn^{2+} , Ni^{2+} , Mg^{2+} , Cu^{2+} have been investigated as well as various pore dimensions by varying the nature of the ligand, e.g. naphthalene-2,6-dicarboxylate, 4,5,9,10-tetrahydropyrene-2,7-dicarboxylate. For MOF-5, reliable measurements made by different laboratories indicate that the maximum uptake of hydrogen is 4.5–5.2 wt.% at 77 K and 50 bar of hydrogen pressure [40]. For room

Fig. 3.15 MOF-5 structure [38]



temperature, the adsorption capacity of MOF-5 is less than 0.2 wt.% at pressures up to 67 bar. The highest value reported is 7 wt.% at 77 K for MOFs having a specific surface area of 3000–4700 m²/g [44, 45].

Neutron powder diffraction of this material revealed that at low-concentration loadings, the ZnO₄ cluster is responsible for most of the adsorption, while the organic linker plays a secondary role only [46]. Inelastic neutron scattering (INS) revealed that a site in the corner of the pore, on the inorganic cluster, ought to be the preferred binding site for hydrogen at low loadings. At higher-loadings, INS indicates the existence of well-defined multiple binding sites for hydrogen within the cavities of MOF-5, with some of these being associated with the organic linking group [47]. A detailed analysis performed by using materials with the same inorganic cluster ZnO₄ and different organic linkers indicates that the binding of hydrogen at the inorganic cluster sites is affected by the nature of the organic link due to differences in their electronic structures [47].

The hydrogen storage capacity of this material is determined by the heat of adsorption (i.e. interaction energy of H₂ molecules) and the specific surface area. Moreover, the interaction of the hydrogen molecules also depends on the pore size, as the presence of small micropores produces an increased adsorbate-adsorbent interaction. At present, the great challenge with this material is to develop new MOFs with an optimum pore size without decreasing the specific surface area.

3.5.1.2 Hydrogen Storage by Chemisorption

The general mechanism of absorption of hydrogen gas by a metal consists in the physisorption of H₂ molecules on the surface, followed by the dissociative chemisorption of individual H atoms. Then, the H atoms diffuse away from the surface into periodic sites (often interstitial) in the metal crystal lattice. Once in the crystal lattice, H atoms can take the form of a random solid solution or an ordered hydride structure with distinct bonding to metal atoms and high volumetric packing density. A fundamental drawback of this method is the necessity to split or recombine the hydrogen molecules and to form chemical bonds with the material. This makes a thermal management of the storage necessary in order to supply or remove the heat

of reaction. Details of the thermodynamic and kinetic properties of hydrides can be found in Part IV, Chap. 16a by J. Huot.

Several compounds have been studied and investigated for hydrogen storage. Their list and a summary of their properties can be found at <http://hydropark.ca.sandia.gov> [48]. Here, selected examples will be presented, including classical hydrides like LaNi_5H_6 and MgH_2 , and advanced storage materials of complex hydrides like alanates and amides or boronates destabilized by partial substitution with Mg.

Classical Hydrides

Metallic hydrides are divided into several types. The most widely studied systems are of the following types:

- A (Mg, V, Ti, ...)
- AB (FeTi, ...)
- A_2B (Mg_2Ni , Mg_2Cu , ...)
- AB_2 (ZrCr_2 , ...)
- AB_5 (LaNi_5 , ...)

where A and B represent that element that is strongly and weakly forming the hydride, respectively. Metallic hydrides are classified either according to the nature of the bond between the metal and hydrogen or according to the temperature at which the decomposition occurs. In the first case, it is distinguished between ionic hydrides, metallic hydrides, and covalent hydrides. In the second case, high-temperature hydrides (MgH_2 , ...) and low-temperature hydrides (LaNi_5H_6 , ...) are distinguished.

La-Ni System

The classical AB_5 hydrides are based on LaNi_5 . The hydriding properties of this material were first reported by Van Vucht et al. in the 1970s [49]. The intermetallic compound is synthesized by induction melting of the pure elements under vacuum or argon atmosphere, followed by annealing at 1073–1473 K [50]. LaNi_5 crystallizes in the hexagonal structure of a CaCu_5 type (space group $P6/mmm$ with La in 1a (0 0 0) and Ni in 2c (1/3 2/3 0) and 3g (1/2 0 1/2)) [50].

Hydrogen can be absorbed into and desorbed from LaNi_5 at nearly atmospheric pressures and 25°C. Absorption/desorption pressure hysteresis is small and the plateaus are rather flat. The enthalpy of formation of LaNi_5H_6 is -30.9 kJ/mol H_2 and the desorption plateau pressure at 25°C is 1.6 atm. The hydrogen storage capacity of this compound is 1.4 wt.% [51]. The capacity loss observed when cycling was commonly attributed to the decomposition of the alloy into lanthanum oxides or hydroxides and nickel particles.

LaNi_5 has very useful properties, but is rather expensive due to the expensive elemental La. Consequently, this element was substituted first by the low-cost rare earth alloy mixed metal (Mm). The most common (Mm) has the following composition (Ce (48–50 wt.%), La (32–34 wt.%), Nd (13–14 wt.%), Pr (4–5 wt.%), other

rare earths (1.5 wt.%). Compared to LaNi_5 , however, the absorption/desorption isotherms of MmNi_5 at 25°C exhibit high pressures of up to 100 atm and hysteresis as can be seen in Fig. 3.16 [52]. As a consequence, other elements were used to partly substitute Mm and Ni in MmNi_5 like $\text{Mm}_{1-x}\text{A}_x\text{Ni}_5$ ($\text{A} = \text{Ca}, \text{Y}, \text{Zr}, \text{etc.}$), $\text{MmNi}_{5-y}\text{B}_y$ ($\text{B} = \text{Co}, \text{Al}, \text{Mn}, \text{Fe}, \text{Cu}, \text{Si}, \text{Ti}, \text{etc.}$) or $\text{Mm}_{1-x}\text{A}_x\text{Ni}_{5-y}\text{B}_y$. These substitutions allow modifying the thermodynamic properties (equilibrium pressure and capacity) of the corresponding hydrides. However, a reduction of the storage capacity and a change of the equilibrium pressure are observed in all cases. Study of the logarithm of the plateau pressure as a function of the intermetallic compound cell volume for various $\text{La}_{1-x}\text{A}_x\text{Ni}_{5-y}\text{B}_y$ at room temperature has shown a linear dependence [53]. As the cell volume can be changed by substitutions, this property allows the plateau pressure of the compound to be adapted to the needs of the application by substituting a proper amount of nickel with other elements like Al or Mn.

AB_5 hydrides and mostly their substitutional derivatives are commercially used in nickel-metal hydride (Ni-MH) batteries. The negative electrode is composed of agglomerated powders of AB_5 alloys, the electrolyte is a concentrated solution of KOH in a small quantity, and the positive electrode is the conventional $\text{NiOOH}/\text{Ni}(\text{OH})_2$ ($E^0 = +0.49\text{ V}$) electrode. More details about the electrochemical performance, cycle life as well as a comparison with different battery families can be found elsewhere [54].

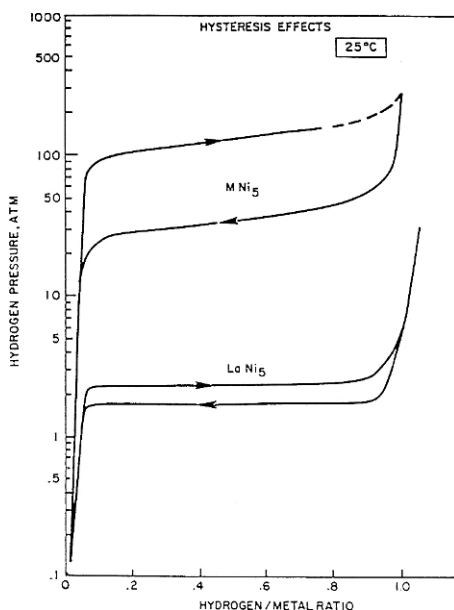


Fig. 3.16 25°C absorption/desorption isotherms for LaNi_5 and MmNi_5 [52]

Mg-based Compounds

Magnesium was considered as a very promising element due to its high storage capacity (7.5 wt.% H) and its low cost. Magnesium absorbs gaseous hydrogen at a temperature above 280°C and a hydrogen pressure above or equal to 10 bar. It is a reversible reaction which is exothermic upon the formation of the hydride and endothermic upon decomposition. The volume expansion occurring during the transformation of the metal to the hydride is in the order of 15%. Magnesium hydride possesses a high thermodynamic stability and very slow kinetics. As a consequence, the focus moved to magnesium alloys (mainly Mg₂Ni, Mg₂Cu, Mg-LaNi₅) which exhibit improved sorption properties, but a decrease in the hydrogen storage capacity [55, 56]. In the 1990s, introduction of ball milling allowed improving drastically the hydrogen absorption/desorption kinetics of pure magnesium. Indeed, ball-milled nanocrystalline magnesium (grain size smaller than 50 nm) could absorb 6 wt.% hydrogen in 120 minutes at 300°C under a hydrogen pressure of 10 bar. Under the same conditions, microcrystalline magnesium (grain size 1 μm) does not absorb any hydrogen [57].

Magnesium hydride can be obtained either by a direct synthesis of the elements at high pressure and a temperature higher than 280°C, by reactive ball milling of magnesium powder (99.9% purity, 100 mesh) at room temperature under a hydrogen pressure of 2 atm [58] or by indirect methods using organic solvents [59, 60] or the ion implantation technique [61]. The β-phase of magnesium hydride crystallizes in the tetragonal structure. The space group is *P4/mnm* and the lattice parameters are $a = 4.5168 \text{ \AA}$ and $c = 3.0205 \text{ \AA}$ with the atomic positions of Mg in (0, 0, 0) and (1/2, 1/2, 1/2) and H in $\pm(X, X, 0)$ and $\pm(X + 1/2, 1/2 - X, 1/2)$ with $X = 0.306$ [62]. In this rutile-type structure each hydrogen atom is in planar coordination with three magnesium atoms. The magnesium atoms are octahedrally coordinated to six hydrogen atoms. The length of the Mg–H bond is 1.95 Å and the H–H distances are 2.49 and 2.76 Å [63, 64]. The β-phase is the stable phase of magnesium hydride. Two metastable phases exist: The γ-MgH₂ phase (obtained by transformation of the β-MgH₂ under high compressive stress) and the δ-MgH₂ phase (obtained by transformation of the β-MgH₂ under high pressure (2.5 to 8 GPa) and high temperature (650 to 800°C)) [65].

Magnesium hydride is a compound which is thermodynamically stable, as the decomposition temperature is around 587 K at a hydrogen pressure of 2.3 bar [66]. The enthalpy and entropy of this compound have been determined by volumetric or gravimetric measurement and using the Van't Hoff diagram. As can be seen in Table 3.1, there is a large scattering of the values of the enthalpy of magnesium hydride formation. In 1999 (by means of a TG-DSC performed under 1 bar of Ar and at a heating rate varying from 1 to 5 K/min), Bogdanovic et al. determined an average enthalpy of desorption of $\Delta_d H(683 \text{ K}) = 74.05 \pm 1.3 \text{ kJ/mol H}_2$ from 14 measurements using a calorimetric method [72]. This implies that a quarter of the energy stored is released as heat during the formation of MgH₂ (exothermic reaction) and should be provided to the system in order to desorb hydrogen (endothermic reaction).

Table 3.1 Enthalpy and entropy values for the formation of magnesium hydride

Enthalpy kJ (mol H ₂) ⁻¹	Entropy J.K ⁻¹ (mol H ₂) ⁻¹	Ref.
-74		[63]
-74.4	135	[66]
-77.4	135	[67]
-70	126	[68]
-85	137	[69]
-80.9		[70]
-74.7		[71]

The reaction between magnesium and gaseous hydrogen should be initiated first by heating the metal to high temperature under vacuum at helium or hydrogen pressure. This is the so-called activation process. In literature, the activation procedure is controversial, as some authors note that magnesium could absorb hydrogen without any treatment [73, 74, 75], while some others suggest that the activation is necessary in the case of magnesium [76, 77]. In general, the formation of magnesium hydride follows a nucleation and growth mechanism. As already stated, hydriding/dehydriding of magnesium is very slow. Therefore, numerous attempts were made to increase the hydrogenation rate and decrease the desorption temperature by modifying several parameters on which the kinetics is highly dependent, such as the shape of the material, the size of the particle, the state of the surface, the thickness of the oxide layer, the presence of impurities, the presence of precursors or additives, etc. To date, the fastest kinetics has been obtained with nanometric powder. Moreover, the hydrogenation rate has been improved by using Pd as catalyst. Indeed, magnesium powder ball-milled with Pd (less than 1 wt.%) absorbs 6 wt.% of hydrogen in 60 minutes at 300°C under a hydrogen pressure of 10 bar without any activation procedure, while 120 minutes were necessary for a powder without palladium [57]. The hydrogenation rate can be further improved by using additives like metals (Ti, Nb, Fe, Co, Ni, Al) [78, 79], non-metals (C, Si) [80], a mixture of metals and non-metals [81], transition metallic oxides (TiO₂, V₂O₅, MnO₂) [82], intermetallic compounds (LaNi₅, FeTi) [83, 84] or mixtures of intermetallics. A review of Mg-based compounds was published by Selvam et al. [85] and Khrussanova [86]. A review of the Mg/Ni system can be found in the paper by Orimo and Fujii [87].

Magnesium hydride is commercially available as a powder, the dehydrogenation/hydrogenation reaction of which also is slow. As in case of magnesium, the kinetics has been improved by ball milling and by doping with a catalyst or an additive. The fastest kinetics has been obtained with the systems (MgH₂ + 5 at.% V) [88] and MgH₂/(TiO₂)_{0.01} [89]. The first system reached 5.5 wt.% H₂ in 500 seconds at 200°C under a hydrogen pressure of 10 bar, the second 6 wt.% H₂ in 300 seconds at 300°C under a hydrogen pressure of 8.4 bar. It was found that the dehydrogenation rate at temperatures between 473 and 573 K was limited by nucleation and two-dimensional growth with an activation energy of 69.5 kJ/mol. At higher temperature, the reaction is interface-controlled with a two-dimensional growth of the forming Mg phase [90]. Structural studies of this system suggest a gateway model,

where hydrogen coming out of magnesium hydride flows through niobium to leave the material [91]. Further improvement has been obtained by doping MgH_2 with 0.5 mol.% Nb_2O_5 . About 7 wt.% of hydrogen were desorbed within 150 seconds at 300°C under a hydrogen pressure of 0.85 MPa [92]. By doping MgH_2 with 1 mol.% Nb_2O_5 by ball milling, Hanada et al. obtained a compound that could absorb more than 5 wt.% of hydrogen at 1 MPa and room temperature [93]. In a recent review paper, Dornheim et al. [94] discussed the role of particle size, fine microstructure, and catalysts. They showed that additives have many favorable effects, such as pinning of grain boundaries, enhancement of hydrogen diffusion, and increases in nucleation rate. Tests in an industrial-size tube vibration mill showed the feasibility of production of hydride-based storage materials on a larger scale.

Advanced Storage Materials

The classical hydrides suffer from a low gravimetric density due to the relatively high mass of the metal atoms. Consequently, the focus of research has moved to systems consisting of light elements, such as Li, Be, B, Na, Mg, Al, Si, K, and Ca. Of these, hydrides from elemental beryllium have been eliminated due to its high toxicity. Among the examples that will be described below are the so-called alanates and the amides or boronates destabilized by partial substitution with Mg. An overview of the progress achieved with these materials is given in the recent review by Orimo et al. [95].

Alanates

Alanates are ternary, salt-like compounds and belong to the so-called “complex hydrides”. Most of the alanates were found to be thermodynamically or kinetically stable at room temperature; they are soluble in many organic solvents and important reducing agents in chemical synthesis. Several alanate compounds like LiAlH_4 (10.54 wt.% H) [96, 97], NaAlH_4 (7.41 wt.% H) [see below], KAlH_4 (5.71 wt.% H) [98], $\text{Mg}(\text{AlH}_4)_2$ (9.27 wt.% H) [99], and $\text{Ca}(\text{AlH}_4)_2$ (7.84 wt.% H) [100] have been synthesized and investigated with respect to hydrogen storage.

Of these candidates, sodium alanate, NaAlH_4 , is the one which has been most widely studied due to its favorable thermodynamic properties which allow for a reversible hydrogen exchange at temperatures around 100°C and its commercial availability [101]. However, hydrogen exchange with the pure compound is kinetically inhibited. These kinetic barriers were first lowered by using transition-metal precursors which were added to the alanate by wet impregnation [102, 103]. Since then, the decomposition reaction has been made reversible under moderate temperature and pressure conditions. Figure 3.17 displays the scheme of the thermal dissociation of pure and catalyzed sodium alanate. The pure, macrocrystalline NaAlH_4 melts at 186°C . Then, the melt starts to decompose and release hydrogen at around 240°C , forming the hexahydride Na_3AlH_6 and elemental Al as solid decomposition products. Pure Na_3AlH_6 decomposes at a temperature above 300°C and releases H_2 , so

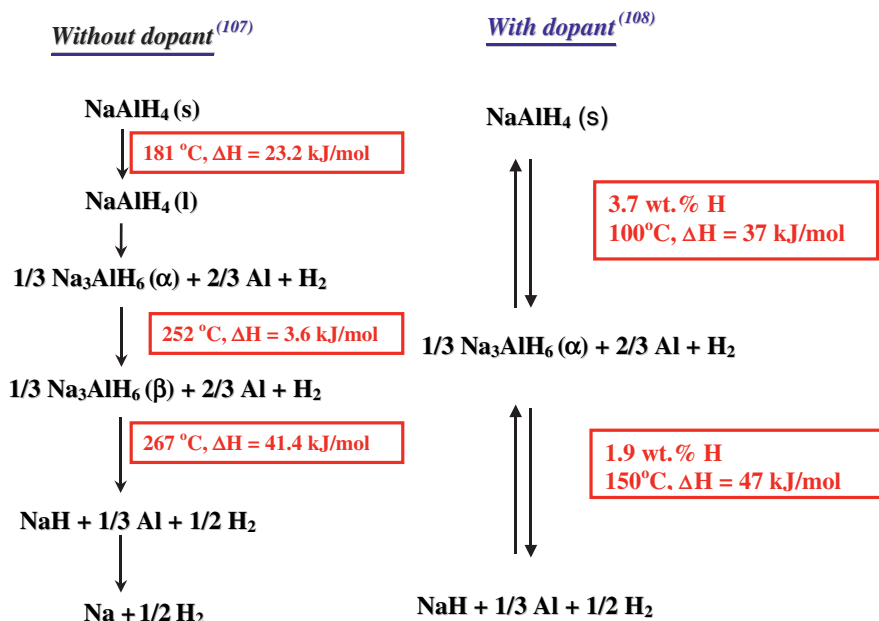


Fig. 3.17 Schematic diagram of the thermal decomposition of pure and doped sodium alanate

that a mixture of two solid phases, NaH and Al, is obtained. The last step is the decomposition of NaH to the elements, which occurs at a temperature above 450°C. Therefore, this step is not considered for practical purposes.

As can be seen, the scheme of a doped sample exhibits significant differences. At first, the reaction is made reversible and from the first two steps, a reversible hydrogen capacity of 5.6 wt.% is expected. The thermal decomposition of doped NaAlH₄ occurs without the melting of the sample. The enthalpy values of 37 and 47 kJ/mol for the first and second step, respectively, were obtained from equilibrium data using the Van't Hoff method. Equilibrium pressures of 1 bar H₂ are reached at 33°C for the first step and at 110°C for the second step. Figure 3.18 displays the crystal structure of NaAlH₄ and Na₃AlH₆. The space group of NaAlH₄ is I 41/a with the lattice parameters of $a = 5.0119 \text{ \AA}$, $b = 5.0119 \text{ \AA}$, $c = 11.3147 \text{ \AA}$ and atomic positions Al (0, 0.25, 0.625), Na (0, 0.25, 0.125), and H (0.2372, 0.3836, 0.5469) [104].

Numerous transition and rare-earth metal catalysts have been investigated as precursors in order to lower the kinetic barriers of NaAlH₄ [105, 106]. Ti-based precursors and, recently, a Ce-based precursor were found to have the best catalytic properties [106, 107, 108, 109]. Moreover, a concentration ranging from 2 to 5 mol.% of Ti or Ce on the basis of TiCl₃, Ti₁₃.6THF, or CeCl₃ has been shown to be a good compromise between the catalytic activity and the loss of storage capacity. The storage material is obtained by adding the precursor to the Na alanate either by wet impregnation or by ball milling. A more detailed description of these

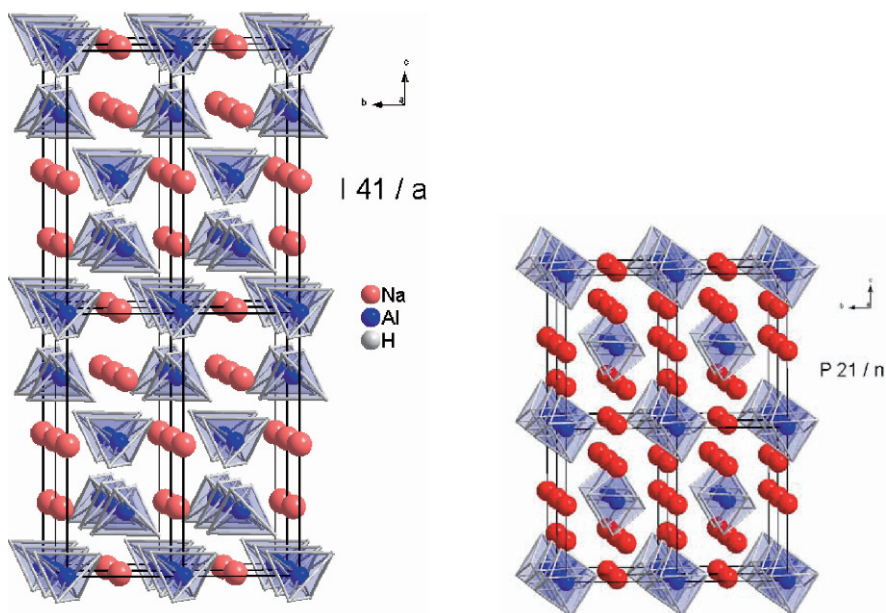


Fig. 3.18 Structure of NaAlH₄ (space group I 41/a, lattice parameters $a = 5.0119 \text{ \AA}$, $b = 5.0119 \text{ \AA}$, $c = 11.3147 \text{ \AA}$, atomic positions Al(0, 0.25, 0.625), Na(0, 0.25, 0.125), H(0.2372, 0.3836, 0.5469)) and Na₃AlH₆ (space group P 21/n, lattice parameters $a = 5.408 \text{ \AA}$, $b = 5.538 \text{ \AA}$, $c = 7.757 \text{ \AA}$, atomic positions Al(0, 0, 0), Na₁(0, 0, 0.5), Na₂(-0.00129, 0.46129, 0.25008), H₁(0.0918, 0.0352, 0.2207), H₂(0.2220, 0.3283, 0.5454), H₃(0.1649, 0.2689, 0.9500))

processes can be found in Part IV, Chap. 15 by Felderhoff. The mechanical alloying has proved to be most efficient in terms of superior kinetic properties. Therefore, this method is widely used to prepare the storage material.

The kinetics of the decomposition reaction of pure sodium alanate and sodium alanate doped with 5 mol.% of Ti on the basis of TiCl₃ or Ti₁₃·6THF is compared in Fig. 3.19. The decomposition of purified NaAlH₄ that has been ball-milled for 30 min and held at 170°C results in the release of the theoretical amount of 5.6 wt.% of hydrogen. The decomposition of the doped material is highly dependent on the nature of the dopant. In fact, 4.5 wt.% of H₂ are released within 700 seconds from sodium alanate doped with Ti colloid, whereas 8000 seconds are needed to reach this state of the reaction when using the TiCl₃-doped sample. The differences between the three materials are drastic. In addition to differences in kinetics, the reversible hydrogen storage capacities differ as well.

The effect of the milling time and cycling under hydrogen on the absorption/desorption kinetics as well as the storage capacity are illustrated for NaAlH₄ doped with 5 mol.% Ti from Ti₁₃·6THF in Figs. 3.20 and 3.21. Decomposition measurements were performed at 150°C under a residual hydrogen pressure of 0.3 bar, absorption was done at 100°C under a hydrogen pressure of 100 bar. Figure 3.21 shows the amount of hydrogen released with desorption time for the

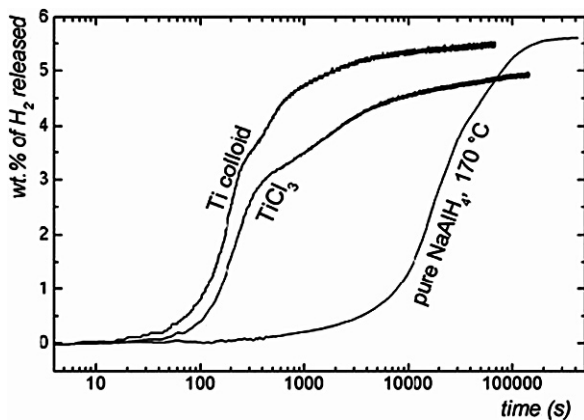


Fig. 3.19 Isothermal decomposition kinetics of the first desorption of pure NaAlH_4 held at 170°C and of Na-alanate doped with 5 mol.% Ti on the basis of TiCl_3 or $\text{Ti}_{13}\cdot 6\text{THF}$ held at 150°C and under a residual hydrogen pressure of 0.3 bar [114]

first (labelled a1d) and the ninth (labelled a9d) dehydrogenation cycle of samples ball-milled for 2 minutes (labelled bm2), 30 minutes (labelled bm30), and 180 minutes (labelled bm180). As can be seen, 5 wt.% H_2 are released in the first desorption cycle within 500 s, 2000 s, and 10,000 s for the samples (bm180), (bm30), and (bm2), respectively. The difference in the desorption times of samples (bm180) and (bm30) mainly results from the kinetics of the second step of the reaction, which

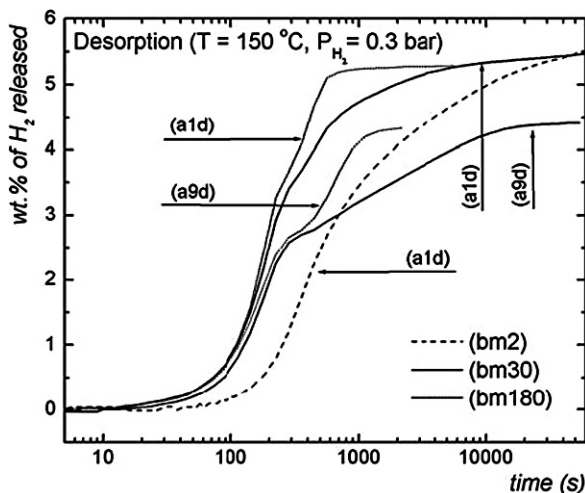


Fig. 3.20 Desorption kinetics of Na-alanate doped with 5 mol.% Ti on the basis of $\text{Ti}_{13}\cdot 6\text{THF}$ at 150°C and a residual pressure of 0.3 bar hydrogen. The first and ninth cycles are presented for samples (bm30) and (bm180). Only the first cycle is shown for sample (bm2) [114]

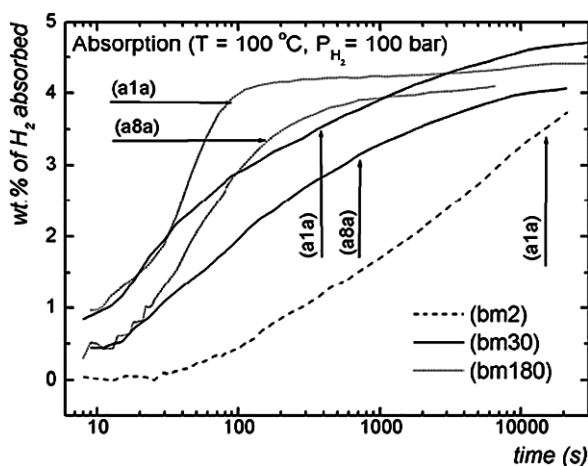


Fig. 3.21 Kinetics of the absorption of Na-alanate doped with 5 mol.% Ti on the basis of $\text{Ti}_{13}\cdot 6\text{THF}$ at 100°C and a hydrogen pressure of 100 bar. The first and ninth cycles are presented for samples (bm30) and (bm180). Only the first cycle is shown for sample (bm2) [114]

is slower in sample (bm30) than in sample (bm180). In the subsequent cycles, the kinetics of both samples decreases and from the fourth cycle, the desorption kinetics does not change significantly. For all samples, 5.5 wt.% of H_2 are released after the first decomposition. Then, the storage capacity decreases continuously and reaches a value of 4.5 wt.% H_2 after 4 cycles for samples (bm180) and (bm30).

Figure 3.21 displays the absorption curves of the first cycle for sample (bm2) and those of the first and ninth absorption cycles for samples (bm30) and (bm180). As for the desorption, kinetics of absorption is faster for sample (bm180) than for sample (bm30). In the first cycle, the sample (bm180) has absorbed 3.5 wt.% of H_2 within 60 s, whereas the sample (bm30) has absorbed 2.5 wt.% only. The absorption kinetics and storage capacity do not change in the first two cycles, while subsequent cycles decrease the kinetics and the amount of hydrogen absorbed by the sample.

Kinetic studies of the different absorption and desorption steps have revealed that the transformation kinetics follows a sigmoidal behavior [110]. The absorption and desorption steps can be fitted with a good agreement by a nucleation and growth model according to the Johnson–Mehl–Avrami theory. It has been shown that transport in the solid is the rate-determining process. This means that diffusion of NaH and Al limits the reaction rate when the hexahydride phase is formed during absorption.

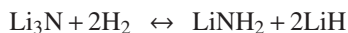
Recent studies on the atomic scale [111, 112, 113] elucidated the state of the dopant in different stages of the dehydrogenation/rehydrogenation reaction. A comparison of the behaviors of the Ti-based precursor-doped materials revealed that most of the Ti species do not remain at the surface upon milling and subsequent cycling, irrespective of the Ti-based precursor used to activate the reversible decomposition reaction of Na alanate [114]. Furthermore, the chemical state of Ti is relevant to the desorption/absorption reaction rate and the storage capacity.

Reduction of Ti species to the metallic state upon ball milling (as occurring for TiCl_3) [112, 113, 114] or during the first absorption reaction (as occurring for the Ti colloid precursor) [114] promotes the formation of small bimetallic entities between Ti and Al. The local environment resulting after several cycles under hydrogen consists of small clusters composed of Ti, surrounded by about 10 Al atoms at $2.80 \pm 0.02 \text{ \AA}$ and a small Ti contribution (around 1 atom) at $3.88 \pm 0.02 \text{ \AA}$. The formation of this nano-scale Ti-Al alloy was correlated with the decrease of the hydrogen storage capacity and the desorption/absorption reaction rate [114]. Considering the structure of NaAlH_4 , XRD analysis by Rietveld refinement indicates that the Bragg positions and the lattice parameters of Ti-doped sodium alanate are preserved [115]. From the refinement of the site occupation factors, the substitution of Ti on the Na site can be excluded. As concerns the substitution of Ti in the Al site, the refinement does not allow a clear statement to be made as for the Na site. Furthermore, there is no vacancy formation in Ti colloid-doped sodium alanate. In situ neutron diffraction experiments performed using uncatalyzed and TiCl_3 -catalyzed NaAlH_4 indicated that the reaction products TiAl_x and NaCl induce grain refinement, while maintaining the small particle size for the decomposition products, high H vacancy densities, and H-D exchange in the catalyzed sample [116].

Some new insights into the reaction have been gained, but the physical and chemical processes involved in hydrogen release and uptake are not yet fully understood. There are still open questions concerning the state of the catalysts as well as the relationships between the structure and the characteristic properties observed with this material. How does the catalyst really work and decrease the thermal activation process? What is physically and chemically happening during cycling?

Combined Systems

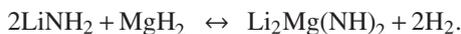
A new way to store hydrogen by using lithium nitrides has been proposed by Chen et al. [117, 118]. The decomposition of Li_3N leads to the formation of a mixture of lithium amide and lithium hydride according to the following reaction:



However, it is more suitable to start with lithium amide in order to increase the reversible capacity. In this case, the decomposition of lithium amide leads to the formation of lithium imide and ammonia at 380°C as follows:



It has been shown that a 1:1 ball-milled LiH-LiNH_2 releases around 5–8 wt.% of H_2 within 3 hours at 210°C . The kinetics was further enhanced to 45 minutes by adding 1mol% of TiCl_3 as catalyst. As the temperature is too high for practical application, intensive research started with respect to the destabilization of LiH-LiNH_2 by the partial substitution of Li by other elements [119]. Among the different mixtures studied, only the 1:2 $\text{MgH}_2\text{-LiNH}_2$ mixture shows a good reversibility with a drop of the storage capacity to 4.5 w.% according to:



Partial substitution of lithium by magnesium lowers the reaction temperature [120], as the reaction enthalpy calculated using the Van't Hoff law is -39 kJ/mol H_2 for the ball-milled 1:2 MgH_2 - LiNH_2 mixture, while it ranges from -45 to -65 kJ/mol H_2 for the decomposition of LiNH_2 . Further improvement was achieved by the ball-milled 2:1 LiH - $\text{Mg}(\text{NH}_2)_2$ mixture with the hydrogen storage capacity reaching 5.6 wt.% and a good reversibility in the 200 – 220°C temperature range. However, one problem of the lithium/nitrogen system is the presence of ammonia in the reactions, as less than 0.1 ppm only is allowed to prevent the poisoning of the PEM fuel cell [2].

Lithium boron hydride is another attractive candidate for hydrogen storage due to its high hydrogen capacity (18.4 wt.%). However, LiBH_4 with an enthalpy estimated to about -70 kJ/mol is too stable for any practical application. An interesting concept is to use a stable boride (MgB_2 , AlB_2) to decrease the heat of formation of boron hydrides [121]. This method was proposed by Vajo et al. [121, 122] and independently by Barkhordarian et al. [123]. In this scheme, the formation of the dehydrogenated alloy MgB_2 can reduce the hydrogenation/dehydrogenation enthalpy by 25 kJ/mol H_2 compared with pure LiBH_4 and the system is reversible according to the following reaction:



Still, the kinetics is too slow, although a catalyst like TiCl_3 is used, and the temperature in the range of 315 – 400°C is too high for any practical applications.

3.5.2 Irreversible Storage Systems

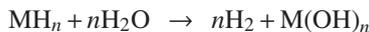
These systems may offer options with high energy densities and potential ease of use, especially if the storage medium is in the liquid form that will allow minimizing the need for infrastructure changes and eliminate the need for large, special containers. In this approach the spent medium should be removed from the vehicle and regenerated with hydrogen either at the fueling station or at a centralized processing facility, as most reactions are irreversible. Therefore, off-board regenerative hydrogen storage technologies may be considered only, if an efficient recycling of the by-products is achieved.

3.5.2.1 Chemical Hydrides

The elements that are of interest in the composition of the hydrides for regenerative off-board storage of hydrogen are Li, Na, Mg, and B. The hydrogen contained in this system can be recovered by two reactions that are exothermic and irreversible:

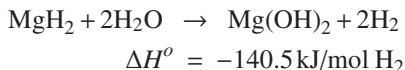
1. Thermal decomposition of the hydride, where the storage material undergoes a chemical decomposition caused by thermal energy.

2. Hydrolysis of the hydride, where the storage material reacts with H_2O , a proton-containing reactant, according to the following reaction:



Simple Hydrides (LiH, NaH, MgH_2 , CaH_2)

The hydrolysis of MgH_2 takes place as follows:



Taking into account the weight of water, a hydrogen storage capacity of 6.5 wt.% of hydrogen may be reached by this system. If the water from the fuel cell is redirected to the chemical hydride, then the yield increases to 15.4 wt.% [124]. The product of the reaction is environmentally benign, but should be regenerated off-board. It has been shown that nanocrystalline magnesium hydride (obtained by ball milling of the polycrystalline material for 20 hours) exhibits a higher conversion rate and a faster kinetics compared to the conventional material. Indeed 54% of the theoretical capacity are released by the polycrystalline material after 20 hours, while 74% are achieved by the nanocrystalline MgH_2 for the same time. After 10 hours of the reaction, however the hydrolysis rate also decreases for the nanocrystalline material due to the formation of a passivation layer. The performance of this material was improved by adding a third metallic element, such as Ca or Li. A significant improvement was achieved with the nanocomposite MgH_2 -Ca 20 at.% milled for 10 hours. Indeed, the hydrolysis reaction was completed in only 4 hours and showed the fastest kinetics compared to MgH_2 -Ca 5 at.% milled for 10 hours.

The advantage of the hydrolysis reaction with these hydrides is that they do not require any catalyst and they possess a high reactivity. However, safety is a concern and most of the time, it is required to use a slurry or encapsulation technology.

Boron Hydrides (MBH_4 with $M = Li, Na, K$)

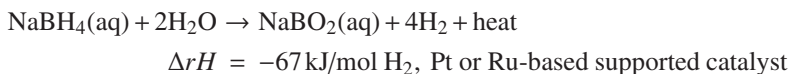
Hydrogen is generated from these compounds by hydrolysis rather than by thermal decomposition because of the high temperature required and the formation of alkali metal in gaseous form that are very corrosive and dangerous in the last step of the decomposition process. Decomposition by reaction with water occurs according to the following equation:



where x depends on the nature of the metal, the temperature, and the composition of the solution.

As can be seen, the metaborates formed bind water and this results in a decrease of the real gravimetric density of the system. Of the three boron hydrides, the reaction of sodium boron hydride solutions is the one studied most by several research groups and companies in the world. Millennium Cell was the leader in developing sodium boron hydride-based energy sources [125].

In the ideal case the catalyzed hydrolysis process of NaBH_4 can be written as follows:



The hydrolysis of NaBH_4 produces 7.3 or 21.2 wt.% depending on whether the water is taken or not taken into account, respectively [126]. Gaseous hydrogen is produced as needed by pumping the fuel over the catalyst or by stopping the pumping of the fuel. Sodium boron hydride is non-flammable, non-explosive, and easy to transport. It is stored at ambient pressure and temperature. Moreover, the reaction that generates the hydrogen is a low-temperature reaction at about 60–80°C. There is no side reaction or volatile by-product. As the reaction is exothermic, there is no need to supply external heat for the reaction to occur. The hydrogen delivered is pure and humidified. The waste borax NaBO_2 is water-soluble and environmentally benign. It can be disposed of or recycled to NaBH_4 on a special site by adding hydrogen and using an appropriate catalyst. A schematic diagram of the on-demand hydrogenation cycle using NaBH_4 for portable fuel cells can be found in Part III, Chap. 12 by Hahn.

The major disadvantages are the cost and the storage in liquid form which is not stable in the long term. In addition, the system capacity should be increased and the energy requirement for regeneration should be lowered. Therefore, novel approaches to an energy-efficient conversion of borates to boron hydride are required.

3.5.2.2 Organic Cycle Compounds

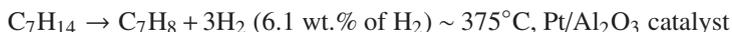
In these compounds hydrogen is stored covalently in an organic liquid carrier, mainly cyclic alkane. A potential advantage is that such a liquid carrier is easily transportable and does not require any water on-board as a co-reactant. In addition, the use of a new type of liquid fuel would not need a major change in today's gasoline infrastructure.

Hydrogen from these compounds is released by interaction with a heated catalyst to form unsaturated aromatic compounds. Hence, dehydrogenation of alkane is an endothermic process, whereas catalytic hydrogenation can be performed at a relatively high temperature, but moderate hydrogen pressure of 7 bar.

Decalin, Methylcyclohexane, *N*-ethyl Carbazole

Liquid cyclic hydrocarbons, such as decalin ($\text{C}_{10}\text{H}_{18}$) and methylcyclohexane (C_7H_{14}) have been studied, as they can release around 6 to 7 wt.% of hydrogen

according to equations. However, a special high-temperature reactor, such as a membrane reactor [127] or isothermal tubular reactor [128], has to be designed. Moreover, a platinum-based or other noble metal catalyst is required to enhance the kinetics of hydrogen evolution. In addition, the generated hydrogen has to be purified most of the time.



To overcome these difficulties, Air product [129] investigated the properties of larger hydrocarbons, mainly polycyclic aromatic compounds and other pi-conjugated molecules, to find a more stable aromatic compound. Taking into account the results of thermodynamic calculations, which indicated that extended polycyclic aromatic hydrocarbons, where one C atom is substituted by one N atom, could lower the enthalpy of dehydrogenation, they selected and investigated the properties of *N*-ethyl carbazole [130]. This compound has a gravimetric hydrogen storage capacity of about 5–7 wt.% and a volumetric capacity of 0.050 kg/l. The enthalpy of dehydrogenation is around 50 kJ/mol H₂. Figure 3.22 displays the hydrogen evolution from *N*-ethyl carbazole after 3 cycles. Dehydrogenation/hydrogenation was carried out with catalysts based on Pd or Ru. Dehydrogenation was performed under a hydrogen pressure of 1 bar and a temperature ramp from 25 to 200°C, the hydrogenation reaction at 170°C under a hydrogen pressure of 82 bar. As can be seen, around 5.5 wt.% of hydrogen can be released in 2 hours and no purification step is necessary. However, the low gravimetric density of this compound calls for the characterization and development of other carbazoles to meet the DOE targets.

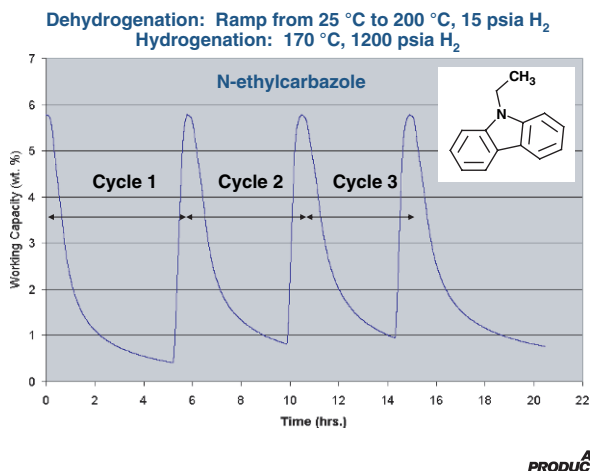


Fig. 3.22 Cyclic desorption of hydrogen from *N*-ethyl carbazole [2]

HYDRNOLTM

Recently, a company from the United States, Asemblon [131], proposed a liquid carrier which stores the hydrogen at ambient temperatures and pressure. The company has named its proprietary liquid carrier HYDRNOLTM, a hydrocarbon-based organic molecule [132]. The Asemblon system consists of four components, the liquid fuel HYDRNOL, the hydrogen release module (which consists of microchannels, a packed bed made of embedded nano-sized catalysts on porous substrates, and nanosprings), the spent fuel recovery module, and the hydrogenation module. In a vehicle, hydrogen is liberated upon demand from HYDRNOL which comes in contact with a hot, high-surface-area catalyst. The depleted HYDRNOL is collected, removed, and transported to a remote site for catalytic hydrogenation.

3.5.3 Outlook

Materials-based approaches, such as solid-state materials or liquids, require less volume than pressurized or cryogenic systems. In addition, safety of on-board vehicular storage of hydrogen is increased, because a tank rupture would not result in large energy releases. Despite extensive effort, however, no material has been found so far, which fulfills the requirements of mobile applications. Hence, new concepts as well as multi-disciplinary approaches are being pursued in order to both increase the reversible storage capacity and the kinetics of hydrogen exchange of systems with suitable thermodynamic properties. On the other hand, metal hydride can be used in limited stationary applications, where weight is not a critical factor and where waste heat is available at the appropriate temperature for hydrogen release.

3.6 Conclusions

Unlike electricity, hydrogen can be stored for long periods of time without significant losses. The three main options that have emerged are compressed hydrogen storage, cryogenic storage, and solid storage. Figure 3.23 displays the actual status of hydrogen storage systems. The compressed hydrogen storage and cryogenic storage are technically available, whereas the third one is still subject of research. As can be seen, none of the current vehicular hydrogen storage systems meets the combined gravimetric, volumetric, and cost targets for either 2010 or 2015. A solution which may be promising is the combination of different storage modes. For example, a tank working under moderate pressure (200 bar) and at low temperature (e.g. liquid nitrogen) allows reaching a storage density close to the 700 bar tank without the technological inconvenience at such a pressure.

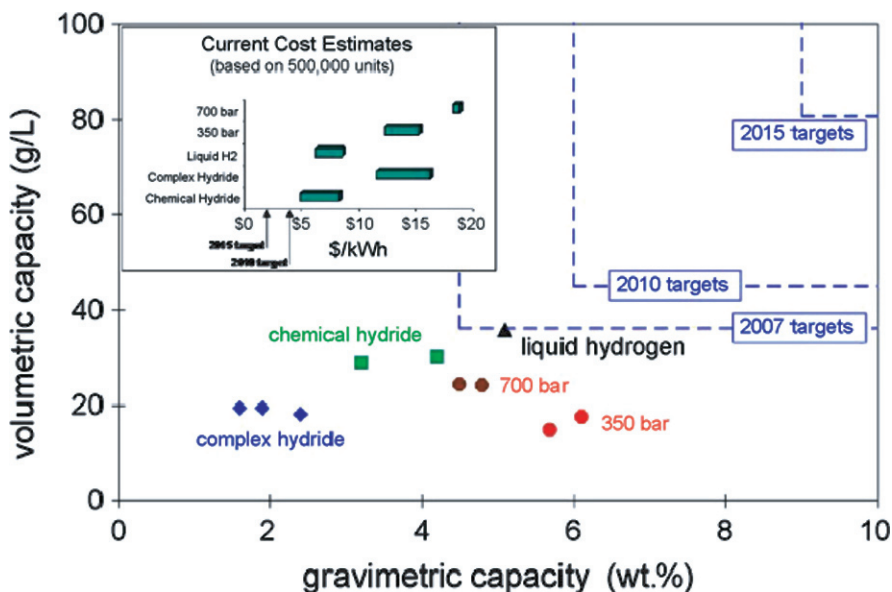


Fig. 3.23 Current status of hydrogen storage systems and cost [2]

A great challenge for future generations of hydrogen-powered vehicles is then the development of lightweight storage systems with conformable tank shapes that can be adapted to the space available in various vehicle structures.

Notes

1. The heat capacity (specific heat) at constant pressure is defined as $C_p = \left(\frac{\partial H}{\partial T}\right)_p$, where H is the enthalpy. The heat capacity at constant volume is $C_v = \left(\frac{\partial U}{\partial T}\right)_v$, where U is the internal energy, T is temperature, and V is the specific volume.
2. The thermal conductivity coefficient relates the transfer of heat through a material via molecular interaction to a temperature gradient across the material.

$$q = -\lambda \times \text{grad}T$$

where q is the heat flux (heat per unit area per unit time), $\text{grad} T$ is the temperature gradient, and λ is the thermal conductivity coefficient.

3. A Joule–Thomson (JT) expansion is an isenthalpic expansion of the gas. The Joule–Thomson coefficient μ represents the drop of the temperature in a JT expansion of a real gas. μ is defined according to the following equation:

$$\mu = -C_p^{-1} \left(\frac{\partial H}{\partial P}\right)_T = \left(\frac{\partial T}{\partial P}\right)_H$$

For certain values of pressure, the coefficient μ is equal to zero. This point is called the inversion point of the Joule–Thomson effect. If the initial temperature of the gas is below the JT

effect inversion temperature, then the gas is cooled during the expansion. Conversely, the gas is warmed during expansion, as it is the case for hydrogen and helium at room temperature.

A Joule–Thomson valve is a component through which a gas is allowed to expand adiabatically, resulting in lowering its temperature.

4. The speed of sound in a gas is defined as follows:

$$c = \sqrt{\gamma \cdot \frac{P}{\rho}}$$

where γ is the isentropic expansion factor (this is the ratio of specific heats of a gas at a constant-pressure to a gas at a constant-volume (C_p/C_v)), p is the pressure and ρ is the density.

5. Hydrogen embrittlement is the process by which various metals, most importantly high-strength steel, become brittle and crack following exposure to hydrogen.

References

1. Encyclopédie des gaz, Air Liquide, Division scientifique, Amsterdam, Elsevier (1976)
2. S. Satyapal, J. Petrovic, C. Read, G. Thomas, and G. Ordaz, “The U.S. department of energy’s national hydrogen storage project: Progress towards meeting hydrogen-powered vehicle requirements”, *Catalysis Today* 120 (2007) 246
3. P. Petit, “Séparation et liquéfaction des gaz”, *Techniques de l’Ingénieur, traité Génie des procédés*, Volume J3 600
4. R. Drnevich, “Hydrogen delivery: liquefaction and compression”, Strategic initiatives for hydrogen delivery workshop, May 7 (2003)
5. <http://www.hydropac.com/>
6. <http://www.pdcmachines.com/>
7. P. Muthukumar, M.P. Maiya, and S.S. Murthy “Experiments on a metal hydride based hydrogen compressor”, *International Journal of Hydrogen Energy*, 30 (2005) 879
8. F. Laurencelle, Z. Dehouche, and J. Goyette, T.K. Bose “Integrated electrolyser-metal hydride compression”, *International Journal of Hydrogen Energy*, 31 (2006) 762
9. X. Wang, R. Chen, Y. Zhang, C. Chen, and Q. Wang “Hydrogen storage alloys for high-pressure suprapure hydrogen compressor”, *Journal of Alloys and compounds*, 420 (2006) 322
10. M. Au and Q. Wang “Rare earth-nickel alloy for hydrogen compression”, *Journal of Alloys and compounds*, 201 (1993) 115
11. Z. Dehouche, N. Grimard, F. Laurencelle, J. Goyette, and T.K. Bose, “Hydride alloys properties investigations for hydrogen sorption compressor”, *Journal of Alloys and compounds*, 399 (2005) 224
12. B. Rohland, K. Eberle, R. Ströbel, J. Scholta, and J. Garche, “Electrochemical hydrogen compressor”, *Electrochimica Acta*, 43(24) (1998) 3841
13. R. Ströbel, M. Oszcipok, M. Fasil, B. Rohland, L. Jörissen, and J. Garche, “The compression of hydrogen in an electrochemical cell based on a PE fuel cell design”, *Journal of Power Sources*, 105 (2002) 208
14. S. Porter, “Hydrogen generation from electrolysis”, *Proton Energy Systems*, May 23 (2005)
15. R. Maruyama, “Electrochemical hydrogen storage into LaNi₅ using a fullerene-based proton conductor”, *Electrochemical and Solid-State Letters*, 5(5) (2002) A89
16. R.S. Irani, *Material Research Society Bulletin* (2002) 680
17. <http://www.qtw.com/>
18. G.E. McIntosh, “Hydrogen liquefiers since 1950”, *Advances in Cryogenic Engineering: Transactions of the Cryogenic Engineering Conference – CEC*, Volume 49 (2004) 9

19. J. Gallarda, "Liquéfaction de l'hydrogène", *Techniques de l'Ingénieur, traité Génie des procédés*, J3, 603
20. M. Bracha, G. Lorenz, A. Patzelt, and M. Wanner, "Large-scale hydrogen liquefaction in Germany", *International Journal of Hydrogen Energy*, 19(1) (1994) 53
21. J. Wolf, "Liquid – Hydrogen Technology for Vehicles", *Material Research Society Bulletin* (2002) 684
22. G. Krainz, G. Bartlok, P. Bodner, P. Casapicola, Ch. Doeller, F. Hofmeister, E. Neubacher, and A. Zieger, "Development of Automotive Liquid Hydrogen Storage Systems", *Advances in Cryogenic Engineering: Transactions of the Cryogenic Engineering Conference – CEC*, 49 (2004) 35
23. B. Kelly, "Liquefaction and pipeline costs", *Hydrogen Delivery Analysis Meeting*, May 2007, Columbia, Maryland, USA
24. M.T. Syed, S.A. Sherif, T.N. Veziroglu, and J.W. Sheffield, "An economic analysis of three hydrogen liquefaction systems", *International Journal of Hydrogen Energy*, 23(7) (1998) 565
25. H. Quack, "Conceptual design of a high efficiency large capacity hydrogen liquefier", *Advances in Cryogenic Engineering: Proceedings of the Cryogenic Engineering Conference*, 47 (2002) 255
26. K. Ohira, K. Nakamichi, and H. Furumoto, "Experimental study on magnetic refrigeration for the liquefaction of hydrogen", *Advances in Cryogenic Engineering*, 45 (2000) 1747
27. A.J. DeGregoria, L.J. Geuling, J.F. Laatsch, and J.R. Rowe, "Test results of an active magnetic regenerative refrigerator", *Advances in Cryogenic Engineering*, 37, Part B (1992) 875
28. C.B. Zimm, E.M. Ludeman, M.C. Severson, and T.A. Henning, "Materials for regenerative magnetic cooling spanning 20 K to 80 K", *Advances in Cryogenic Engineering*, 37, Part B (1992) 883
29. K.A. Gschneidner, Jr., H. Takeya, J.O. Moorman, V.K. Pecharsky, S.K. Malik, and C.B. Zimm "New magnetic refrigeration materials for the liquefaction of hydrogen", *Advances in Cryogenic Engineering*, 39, Part B (1994) 1457
30. K.A. Gschneidner, Jr., V.K. Pecharsky, and S.K. Malik, "The $(\text{Dy}_{1-x}\text{Er}_x)\text{Al}_2$ alloys as active magnetic regenerators for magnetic refrigeration", *Advances in Cryogenic Engineering*, 42 (1996) 475
31. M.A. Richard, A.M. Rowe, and R. Chahine, "Magnetic refrigeration: Single and multimaterial active magnetic regenerator experiments", *Journal of Applied Physics*, 95(4) (2004) 2146
32. A. Zuettel, P. Sudan, Ph. Mauron, T. Kiyobayashi, Ch. Emmenegger, and L. Schlapbach, "Hydrogen storage in carbon nanostructures", *International Journal of Hydrogen Energy*, 27 (2002) 203
33. M.G. Nijkamp, J.E. Raaymakers, A.J. van Dillen, and K.P. deJong, "Hydrogen storage using physisorption-materials demand", *Applied Physics A*, 72 (2001) 619
34. E. Poirier, R. Chahine, P. Bénard, D. Cossement, L. Lafi, E. Melançon, T.K. Bose, and S. Désilets, "Storage of hydrogen on single-walled carbon nanotubes and other carbon structures", *Applied Physics A*, 78 (2004) 961
35. B. Panella and M. Hirscher, "Hydrogen adsorption in different carbon nanostructures", *Carbon*, 43 (2005) 2209
36. M Hirscher and B. Panella "Large surface area nanostructures for hydrogen storage", *Annales de Chimie Science des Matériaux*, 30(5) (2005) 519
37. M. Eddaoudi, J. Kim, N. Rosi, D. Vodak, J. Wachter, M. O'Keeffe, and O.M. Yaghi, "Systematic design of pore size and functionality in isoreticular MOFs and their application in methane storage", *Science*, 295 (2002) 469
38. O.M. Yaghi, M. O'Keeffe, N.W. Ockwig, H.K. Chae, M. Eddaoudi, and J. Kim, "Reticular synthesis and the design of new materials", *Nature*, 423 (2003) 705
39. J.L.C. Roswell, A.R. Milward, K.S. Park, and O.M. Yaghi, "Hydrogen sorption in functionalized metal-organic framework", *Journal of the American Chemical Society*, 126 (2004) 5666
40. B. Panella and M. Hirscher, "Hydrogen physisorption in metal-organic porous crystals", *Advanced Materials*, 17(5) (2005) 538
41. M Hirscher and B. Panella, "Hydrogen storage in metal-organic frameworks", *Scripta Materialia*, 56 (2007) 809

42. N. Texier-Mandoki, J. Dentzer, T. Piquero, S. Saadallah, P. David, and C. Vix-Guterl, "Hydrogen storage in activated carbon materials: Role of nanoporous texture", *Carbon*, 42 (2004) 2735
43. R. Gadiou, S. Saadallah, T. Piquero, P. David, J. Parmentier, and C. Vix-Guterl, "The influence of textural properties on the adsorption of hydrogen on ordered nanostructured carbons", *Microporous and Mesoporous Materials*, 79 (2005) 121
44. A.G. Wong-Foy, A.J. Matzer, and O.M. Yaghi, "Exceptional H₂ saturation uptake in microporous metal-organic frameworks", *Journal of the American Chemical Society* 128 (2006) 3494
45. D.J. Collins and H.-C. Zhou, "Hydrogen storage in metal-organic frameworks", *Journal of Material Chemistry*, 17 (2007) 3154
46. T. Yildirim and M.R. Hartman, "Direct observation of hydrogen adsorption sites and nanocage formation in metal-organic frameworks", *Physical Review Letters*, 95 (2005) 215504
47. J.L.C. Roswell, J. Eckert, and O.M. Yaghi, "Characterization of H₂ binding sites in prototypical metal-organic frameworks by inelastic neutron scattering", *Journal of American Chemical Society*, 127 (2005) 14904
48. G. Sandrock and G. Thomas, "The IEA/DOE/SNL on-line hydride databases", *Applied Physics A*, 72(2) (2001) 153
49. J.H.N. Van Vucht, F.A. Kuijpers, and H.C.A.M. Bruning, *Philips Research Report*, 25 (1970) 133
50. R. Cerny, J.M. Joubert, M. Latroche, A. Percheron-Guégan, and K. Yvon, *Journal of Applied Crystallography*, 33 (2000) 997
51. C. Lartigue, A. Percheron-Guégan, J.C. Achard, and F. Tasset, *Journal of the Less Common Metals*, 75 (1980) 23
52. G. Sandrock, "Hydrogen-metal systems" in *Hydrogen Energy System*, Y. Yürüm (ed.), Kluwer Academic Publishers, Netherlands (1995) 135
53. F. Cuevas, J.M. Joubert, M. Latroche, and A. Percheron-Guégan, "Intermetallic compounds as negative electrodes of Ni/MH batteries", *Applied Physics A*, 72 (2001) 225
54. J.M. Joubert, M. Latroche, and A. Percheron-Guégan, "Metallic hydrides II: Materials for electrochemical storage", *Material Research Society Bulletin* September (2002) 694
55. G. Liang, "Synthesis and hydrogen storage properties of Mg-based alloys", *Journal of Alloys and Compounds*, 370 (2004) 123
56. J.J. Reilly, "Synthesis and properties of useful metal hydrides", in *Hydrides for energy storage*, A.F. Andresen and A.J. Maeland (eds), Pergamon press, Oxford (1978) 301
57. A. Zaluska, L. Zaluski, and J.O. Ström-Olsen, "Nanocrystalline magnesium for hydrogen storage", *Journal of Alloys and Compounds*, 288 (1999) 217
58. Y. Chen and J.S. William, "Formation of metal hydrides by mechanical alloying" *Journal of Alloys and Compounds*, 217 (1995) 181
59. H. Imamura, M. Kawahigashi, and S. Tsuchiya "Exceptionally active magnesium for hydrogen storage: Solvated magnesium clusters formed in low temperature matrices", *Journal of the Less Common Metals*, 95 (1983) 157
60. B. Bogdanovic, "Magnesium hydride: A homogeneous-catalysed synthesis and its use in hydrogen storage", *International Journal of Hydrogen Energy*, 9 (1984) 937
61. A. Altmann and T. Schober, "Hydrides in Mg and Ti produced by hydrogen ion implantation", *Scripta Metallurgica and Materialia*, 25(3) (1991) 723
62. A.S. Pedersen, "Magnesium (Beryllium) and alkaline earth (calcium, strontium and barium) hydrides", in *Solid State Phenomena*, E.A. Lewis and A. Aladjem (eds), Scitec Publications volume 49–50 (1996) 46
63. H. Ellinger, C.E. Holley, B.B. McInteer, D. Pavone, R.M. Potter, E. Staritsky, and W.H. Zachariassen, "The preparation and some properties of magnesium hydride", *Journal of American Chemical Society*, 77 (1955) 2647
64. W.H. Zachariassen, C.E. Holley, and J.F. Stamper, "Neutron diffraction study of magnesium hydride", *Acta Crystallographica*, 16 (1963) 352

65. A. San-Martin and F.D. Manchester, "The H-Mg (Hydrogen-Magnesium) system", *Bulletin of Alloy Phase diagrams*, 8(5) (1987) 431
66. J.F. Stamper, Jr., C.E. Holley, Jr., and J.F. Suttle, "The magnesium-hydrogen system", *Journal of American Chemical Society*, 82 (1960) 3504–3508
67. B. Tanguy, J.L. Soubeyroux, M. Pezat, J. Portier, and P. Hagemuller, "Amélioration des conditions de synthèse de l'hydrure de magnésium à l'aide d'adjuvants", *Material Research Bulletin*, 11, (1976) 1441–1448
68. A.S. Pedersen, J. Kjøller, B. Larsen, B. Vigeholm, and J.A. Jensen, "Magnesium for hydrogen storage", *International Journal of Hydrogen Energy*, 8 (1983) 205–211
69. L. Belkbir, E. Joly, and N. Gerard, "Comparative study of the formation-decomposition mechanisms and kinetic in LaNi_5 and magnesium reversible hydride", *International Journal of Hydrogen Energy*, 6 (1981) 2145–2156
70. B. Bogdanovic, A. Ritter, B. Spliethoff, and K. Straßburger, "A process steam generator based on the high temperature magnesium hydride/magnesium heat storage system", *International Journal of Hydrogen Energy*, 20 (1995) 811–822.
71. G. Friedlmeier and M. Groll, "Experimental analysis and modelling of the hydriding kinetics of Ni-doped and pure Mg", *Journal of Alloys and compounds*, 253–254 (1997) 550–555,
72. B. Bogdanovic, K. Bohmhammel, B. Christ, A. Reiser, K. Schlichte, R. Vehlen, and U. Wolf, "Thermodynamic investigation of the magnesium-hydrogen system", *Journal of Alloys and compounds*, 282 (1999) 84–92
73. B. Vigeholm, J. Kjøller, and B. Larsen, "Magnesium for hydrogen storage", *Journal of the Less Common Metals*, 74 (1980) 341–350
74. B. Vigeholm, "Magnesium as an energy material", *Proceedings – World Magnesium Conference, Proceedings – 41st World Magnesium Conference, London*, pp. 59–63
75. A. Zaluska, L. Zaluski, and J.O. Ström-Olsen, "Nanocrystalline magnesium for hydrogen storage", *Journal of Alloys and Compounds*, 288 (1999) 217–225
76. A.S. Pedersen, J. Kjøller, B. Larsen, and B. Vigeholm, "On the hydrogenation mechanism in magnesium I", in *Hydrogen energy progress V, Proceedings of the 5th World Hydrogen Energy Conference, Toronto 15–20 July 1984*, ed. by T.N. Veziroglu and J.B. Taylor, Pergamon Press, New-York, pp. 1269–1277
77. C.P. Chen, B.H. Liu, Z.P. Li, and J. Wu, "The activation mechanism of Mg-based hydrogen storage alloys", *Zeitschrift für Physikalische Chemie B*, 181 (1993) 259–267
78. E. Ivanov, I. Konstantchuk, A. Stepanov, and V. Boldyrev "Magnesium mechanical alloys for hydrogen storage", *Journal of the Less Common Metals*, 131 (1987) 25–29
79. S. Bouaricha, J.P. Dodelet, D. Guay, J. Huot, S. Boily, and R. Schulz, "Hydriding behavior of Mg-Al and leached Mg-Al compounds prepared by high-energy ball milling", *Journal of Alloys and Compounds*, 297 (2000) 282–293
80. H. Imamura, S. Tabata, Y. Takesue, Y. Sakata, and S. Kamazaki, "Hydriding-dehydriding behavior of magnesium composites obtained by mechanical grinding with graphite carbon", *International Journal of Hydrogen Energy*, 25 (2000) 837–843
81. M. Khrussanova, J.-L. Bobet, M. Terzieva, B. Chevalier, D. Radev, P. Peshev, and B. Darriet, "Hydrogen storage characteristics of magnesium mechanically alloyed with $\text{YNi}_{5-x}\text{Al}_x$ ($x = 0, 1$ and 3)", *Journal of Alloys and Compounds*, 307 (2000) 283–289
82. P. Wang, A.M. Wang, H.F. Zhang, B.Z. Ding, and Z.Q. Hu, "Hydrogenation characteristics of Mg-TiO₂ (rutile) composite", *Journal of Alloys and Compounds*, 313, (2000) 218–223
83. M. Terzieva, M. Khrussanova, and P. Peshev, "Hydriding and dehydriding characteristics of Mg-LaNi₅ composite materials prepared by mechanical alloying", *Journal of Alloys and Compounds*, 267 (1998) 235–239
84. G. Liang, S. Boily, J. Huot, A. Van Neste, and R. Schulz, "Hydrogen absorption properties of a mechanically milled Mg-50 wt.% LaNi₅ composite", *Journal of Alloys and Compounds*, 268, (1998) 302–307
85. P. Selvam, B. Viswanathan, C.S. Swamy, and V. Srinivasan, "Magnesium and magnesium alloy hydrides", *International Journal of Hydrogen Energy*, 11(3) (1986) 169–192
86. M. Khrussanova, "Metal alloy hydrides for hydrogen storage", *Bulgarian Academy of Science*, 19(3), (1986) 358–373

87. S. Orimo and H. Fujii, "Materials science of Mg-Ni-based new hydrides", *Applied Physics A*, 72(2) (2001) 167–186
88. G. Liang, J. Huot, S. Boily, A. Van Neste, and R. Schulz, "Hydrogen storage properties of the mechanically milled MgH_2 -V nanocomposite", *Journal of Alloys and Compounds*, 291, (1999) 295–299
89. W. Oelerich, T. Klassen, and R. Bormann, "Metal oxides as catalysts for improved hydrogen sorption in nanocrystalline Mg-based materials", *Journal of Alloys and Compounds*, 315 (2001) 237–242
90. G. Liang, J. Huot, S. Boily, and R. Schulz, "Hydrogen desorption kinetics of a mechanically milled $\text{MgH}_2 + 5\text{at.}\% \text{ V}$ nanocomposite", *Journal of Alloys and Compounds*, 305 (2000) 239.
91. J.F. Pelletier, J. Huot, M. Sutton, R. Schulz, A.R. Sandy, L.B. Lurio, and S.G.J. Mochrie, "Hydrogen desorption mechanism in $\text{MgH}_2 - \text{Nb}$ nanocomposite", *Physical review B*, 63 (2000) 521
92. G. Barkhordarian, T. Klassen, and R. Bormann, *Scripta Materialia*, 49 (2003) 213
93. N. Hanada, T. Ichikawa, S. Hino, and H. Fujii, "Remarkable improvement of hydrogen sorption kinetics in magnesium catalyzed with Nb_2O_5 ", *Journal of Alloys and Compounds*, 420 (2000), 46–49
94. M. Dornheim, N. Eigen, G. Barkhordarian, T. Klassen, and R. Bormann, *Advanced Engineering Materials*, 8(5) (2006) 377–385
95. S.I. Orimo, Y. Nakamori, J.R. Eliseo, A. Züttel, and C.M. Jensen, "Complex Hydrides for Hydrogen Storage", *Chemical Reviews*, 107 (2007) 4111–4132
96. J. Chen, N. Kuriyama, Q. Xu, H.T. Takeshita, and T. Sakai, "Reversible hydrogen storage via titanium-catalyzed LiAlH_4 and Li_3AlH_6 ", *Journal of Physical Chemistry B*, 105 (2001) 11214–11220
97. H. Morioka, K. Kakizaki, S.-C. Chung, and A. Yamada, "Reversible hydrogen decomposition of KAlH_4 ", *Journal of Alloys and Compounds*, 353 (2003) 310–314
98. M. Fichtner, O. Fuhr, and O. Kircher, "Magnesium alanate – a material for reversible hydrogen storage?", *Journal of Alloys and Compounds*, 356–357 (2003) 418–422
99. M. Mamatha, B. Bogdanovic, M. Felderhoff, A. Pommerin, W. Schmidt, F. Schüth, and C. Weidenthaler, "Mechanochemical preparation and investigation of properties of magnesium, calcium and lithium-magnesium alanates", *Journal of Alloys and Compounds*, 407 (2006) 78–86
100. http://www.albemarle.com/Products_and_services/Fine_chemicals/
101. P. Claudy et al., "Étude du comportement thermique du tetrahydroaluminate de sodium NaAlH_4 et de l'hexahydroaluminate de sodium Na_3AlH_6 de 298 a 600 K", *Thermochimica Acta*, 8 (1980) 75
102. B. Bogdanovic and M. Schwickardi, "Ti-doped alkali metal aluminium hydrides as potential novel reversible hydrogen storage materials", *Journal of Alloys and Compounds*, 253–254, (1997) 1–9
103. B.C. Hauback, H.W. Brinks, C.M. Jensen, K. Murphy, and A.J. Maeland, "Neutron diffraction structure determination of NaAlD_4 ", *Journal of Alloys and Compounds*, 358 (2003) 142–145
104. D.L. Anton, "Hydrogen desorption kinetics in transition metal modified NaAlH_4 ", *J. Alloys and Compounds*, 356 (2003) 400
105. B. Bogdanovic, G. Sandrock, "Catalized complex Metal Hydrides", *MRS bulletin*, 712 (2002)
106. M. Fichtner, O. Fuhr, O. Kircher, and J. Rothe, "Small Ti clusters for catalysis of hydrogen exchange in NaAlH_4 ", *Nanotechnology*, 14 (2003) 778
107. B. Bogdanovic, M. Felderhoff, S. Kaskel, A. Pommerin, K. Schlichte, and F. Schüth, "Improved hydrogen storage properties of Ti-doped sodium alanate using titanium nanoparticles as doping agents", *Advanced Materials*, 15 (2003) 1012
108. B. Bogdanovic, M. Felderhoff, A. Pommerin, F. Schüth, and N. Spielkamp, "Advanced hydrogen storage materials based on Sc-, Ce-, and Pd-doped NaAlH_4 ", *Advanced Materials*, 18 (2006) 1198

109. O. Kircher and M. Fichtner, "Hydrogen exchange kinetics in NaAlH₄ catalyzed in different decomposition states", *Journal of Applied Physics*, 95(12) (2004) 7748
110. A. Léon, O. Kircher, J. Rothe, and M. Fichtner, "Chemical state and local structure around titanium atoms in NaAlH₄ doped with TiCl₃ using X-ray absorption spectroscopy", *The Journal of Physical Chemistry B*, 108 (2004) 16372
111. J. Graetz, J.J. Reilly, J. Johnson, A.Y. Ignatov, and T.A. Tyson, "X-ray absorption study of Ti-activated sodium aluminum hydride", *Applied Physics Letters*, 85 (2004) 500
112. M. Felderhoff, K. Klementiev, W. Grünert, B. Spielthoff, B. Tesche, J.M. Bellosta von Colbe, B. Bogdanovic, M. Härtel, A. Pommerin, F. Schüth, and C. Weidenthaler, "Combined TEM-EDX and XAFS studies of Ti-doped sodium alanate", *Physical Chemistry Chemical Physica*, 6 (2004) 4369
113. A. Léon, O. Kircher, J. Röthe, S. Dieter, and M. Fichtner, "Evolution of the local structure around Ti atoms in NaAlH₄ doped with TiCl₃ or small Ti clusters (Ti₁₃ · 6THF) by ball milling", *Journal of Physical Chemistry B*, 110 (2006) 1192
114. P. Canton, M. Fichtner, C. Frommen, and A. Léon "Synchrotron X-ray studies of Ti-doped NaAlH₄", *Journal of Physical Chemistry B*, 110 (2006) 3051
115. S. Singh, S.W.H. Eijt, J. Huot, W.A. Kockelmann, M. Wagemaker, and F.M. Mulder, "The TiCl₃ catalyst in NaAlH₄ for hydrogen storage induces grain refinement and impacts on hydrogen vacancy formation", *Acta Materialia* 55 (2007) 5549
116. P. Chen, Z. Xiong, J. Luo, J. Lin, and K.L. Tan, "Interaction of hydrogen with metal nitrides and imides", *Nature*, 420 (2002) 302–304
117. P. Chen, Z. Xiong, G. Wu, Y. Liu, J. Hu, and W. Luo, *Scripta Materialia*, 56 (2007) 817
118. H. Fujii and T. Ichikawa, "Recent development on hydrogen storage materials composed of light elements", *Physica B*, 383 (2006) 45–48
119. W. Luo, "(LiNH₂ – MgH₂): A viable hydrogen storage system", *Journal of Alloys and Compounds*, 381 (2004) 284–287
120. G.L. Soloveichik, "Metal borohydrides as hydrogen storage materials", *Materials Matters*, 2 (2007) 11–14
121. J.J. Vajo, S.L. Skeith, and F. Martens, "Reversible storage of hydrogen in destabilized LiBH₄", *Journal of Physical Chemistry B*, 109 (2005) 3719–3722
122. J.J. Vajo and G.I. Olson, "Hydrogen storage in destabilized chemical systems", *Scripta Materialia*, 56 (2007) 829
123. G. Barkhordarian, T. Klassen, M. Dornheim, and R. Bormann, "Unexpected kinetic effect of MgB₂ in reactive hydride composites containing complex borohydrides", *Journal of Alloys and Compounds*, 440 (2007) L18–L21
124. J. Huot, G. Liang, and R. Schulz, "Magnesium-based nanocomposites chemical hydrides", *Journal of Alloys and Compounds*, 353 (2003) L12
125. S.C. Amendola, "Process for synthesizing borohydride compounds", US patent 6524542 (2003)
126. <http://www.millenniumcell.com>
127. P. Ferreira-Aparacio, I. Rodriguez-Ramos, and A. Guerrero-Ruiz, "Pure hydrogen production from methylcyclohexane using a new high performance membrane reactor", *Chemical Communications* 2002(18) (2002) 2082
128. G. Bustamante, Y. Swesi, I. Pitault, V. Meille, and F. Heurtaux, "A hydrogen storage and transport mean", *Proceedings International Energy Congress and Exhibition IHEC* (2005) Turkey
129. <http://www.airproducts.com>
130. A. Cooper and G. Pez, "Development of new carbon-based sorbent systems for an effective containment of hydrogen", DOE Annual Merit Review Presentation (2005), available at: http://www.hydrogen.energy.gov/annual_progress05_storage.html
131. <http://www.asemblon.com>
132. E.D. Naeemi, D. Graham, and B.F. Norton, "Introducing HYDRNOL TM: Organic liquid storage for hydrogen", *Sigma Aldrich*, 2(2) (2007) 23